Applications of topology optimization techniques in seismic design of structure

Ghabraie, Kazem 2012, Applications of topology optimization techniques in seismic design of structure. In Plevris, Vagelis, Mitropoulou, Chara Ch. and Lagaros, Nikos D. (ed), *Structural seismic design optimization and earthquake engineering: formulations and applications*, IGI Global, Hershey, Pa., pp.232-268.

DOI: 10.4018/978-1-4666-1640-0.ch010

Chapter 10
Applications of Topology Optimization Techniques in Seismic Design of Structure

Kazem Ghabraie
University of Southern Queensland, Australia

ABSTRACT

During the last two decades, topology optimization techniques have been successfully applied to a wide range of problems including seismic design of structures. This chapter aims to provide an introduction to the topology optimization methods and a review of the applications of these methods in earthquake engineering. Two well-established topology optimization techniques are introduced. Several problems including eigenfrequency control of structures, compliance minimization under periodic loading, and maximizing energy absorption of passive dampers will be addressed. Numerical instabilities and approaches to overcome them will be discussed. The application of the presented approaches and methods will be illustrated using numerical examples. It will be shown that in seismic design of structures, topology optimization methods can be useful in providing conceptual design for structural systems as well as detailed design of structural members.

1. INTRODUCTION

Solving optimization problems is an inherent part of engineering design where one seeks the best design to minimize or maximize an objective function subject to some constraints. In structural optimization, depending on the nature of the design variables, three different optimization categories can be recognized. *Sizing optimization* arises when the design variables are connected to the dimensions of the elements. It can be useful where the layout and the shapes of the members

DOI: 10.4018/978-1-4666-1640-0.ch010

Figure 1. The three levels of structural optimization: top) sizing optimization; middle) shape optimization; bottom) topology optimization

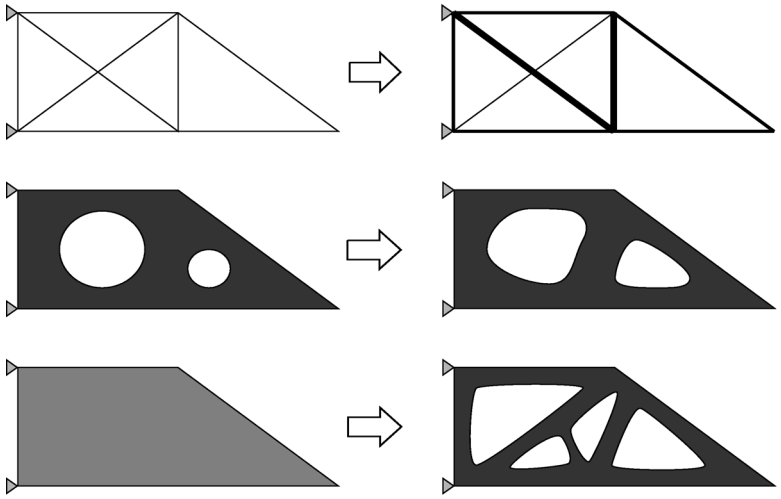

are known and it is desired to find the optimum dimensions. On another level, one can choose the design variables to control the shape of the boundaries of the members. Such selection will lead to *shape optimization*. If the overall layout of the members is known and it is already decided where to put each member, in order to find the best shapes of the members, one can use shape optimization. In order to optimize the topology, connectivity, or layout of a system, *topology optimization* techniques should be used. In topology optimization the design variables control the topology and connectivity of the design. Figure 1 schematically illustrates these three categories of structural optimization.

Starting from topology optimization and feeding the results to shape and sizing optimization routines will generally result in far greater savings than merely using shape and sizing optimization. Topology optimization techniques can thus be considered as important and powerful tools in hand of design engineers.

In this chapter we review the application of topology optimization techniques in seismic design of structures. We start with a brief review of the history of topology optimization. Then we focus on two general optimization problems in seismic design of structures, the eigenvalue optimization problem and the problem of maximizing the energy absorption.

2. TOPOLOGY OPTIMIZATION

Initially addressed by Culmann (1866), the layout optimization problem is not quite new. The interesting work of Michell (1904) laid down the principles of topology optimization of structures more than a century ago. After that, the field remained untouched for nearly seven decades until Prager and Rozvany improved and generalized the Michell's theory (e.g. refer to Prager 1969, 1974 and Rozvany 1972a,b). Yet the field didn't attract much attention until Bendsøe and Kikuchi (1988) proposed a finite element-based numerical method for topology optimization of continuum structures. Usually referred to as the *homogenization method*, this approach soon became a basis upon which other topology optimization techniques have been developed.

In their approach, Bendsøe and Kikuchi considered special microstructures as the building cells of the structure and employed the homogenization method to find the macro-scale properties of the cells in terms of their micro-scale dimensions. By considering the dimensional properties of the microstructures as design variables, they reduced the topology optimization of the structure to sizing optimization of its microstructures.

Using the idea behind the homogenization method, Bendsøe (1989) introduced a simpler approach to optimize the topology of structures. In this new approach instead of using the microstructures and homogenization, Bendsøe proposed an artificial material interpolation scheme relating the material properties of the elements to their relative density. After Rozvany et al. (1992), this approach is referred to as 'Solid Isotropic Microstructures with Penalization (SIMP)'. The SIMP approach is now one of the most established and popular methods in topology optimization.

A simple FE-based topology optimization technique was later proposed by Xie and Steven (1993). Named Evolutionary Structural Optimization (ESO), the technique was based on the idea of evolving the structure towards an optimum design by progressively removing its inefficient elements. The Bi-directional ESO (BESO) was the main successor of the ESO method. Initially introduced by Querin (1997), Querin et al. (1998) and Yang et al. (1999a), the BESO algorithm was capable of adding as well as removing elements. This method is now a well-known topology optimization technique which is widely used due to its clear topology results and ease of application.

The SIMP and BESO techniques will be detailed and used in later sections of this chapter. In the next section we investigate the equation of motion of a structural system to find out which parameters shape the responses of structures under dynamic loads.

3. STRUCTURAL RESPONSES UNDER DYNAMIC LOADS

Consider the equation of motion for a finite element discretized linear system

$$\mathbf{M}\ddot{\mathbf{u}} + \mathbf{C}\dot{\mathbf{u}} + \mathbf{K}\mathbf{u} = \mathbf{p} \tag{1.1}$$

where $\mathbf{M}$, $\mathbf{C}$ and $\mathbf{K}$ are mass, damping and stiffness matrices respectively and $\mathbf{u}$ and $\mathbf{p}$ are time-dependent vectors of nodal displacement and nodal force respectively, i.e., $\mathbf{u} \equiv \mathbf{u}(t)$ and $\mathbf{p} \equiv \mathbf{p}(t)$. We assume a classical damping (Chopra 1995), for example Reyliegh damping of the form

$$\mathbf{C} = a_M\mathbf{M} + a_K\mathbf{K} \tag{1.2}$$

where a_M and a_K are constants.

We now expand the displacements in terms of modal contributions

$$\mathbf{u}(t) = \sum_{r=1}^{N_d} q_r(t)\boldsymbol{\varphi}_r \tag{1.3}$$

where N_d is the number of degrees of freedom and

$$q_r(t) = C_r \cos\omega_r t + S_r \sin\omega_r t, \qquad r = 1,\ldots,N_d \tag{1.4}$$

are harmonic functions and C_r and S_r are constants of integration associated with the rth degree of freedom. The natural frequencies ω_r and natural modes $\boldsymbol{\varphi}_r$ are solutions of the following eigenvalue problem

$$\mathbf{K}\boldsymbol{\varphi}_r = \omega_r^2\mathbf{M}\boldsymbol{\varphi}_r \tag{1.5}$$

which represents the free vibration of the undamped system. For simplicity, we further require that the modes are $\mathbf{M}$-orthonormal, i.e.,

$$\boldsymbol{\varphi}_n^T \mathbf{M} \boldsymbol{\varphi}_r = \delta_{nr}, \qquad n, r = 1, \ldots, N_d \tag{1.6}$$

where δ_{nr} is the Kroneker's delta which equals 1 for $n = r$ and 0 otherwise. Premultiplying Equation (1.5) by $\boldsymbol{\varphi}_n^T$ and using Equation (1.6) we get

$$\boldsymbol{\varphi}_n^T \mathbf{K} \boldsymbol{\varphi}_r = \omega_r^2 \delta_{nr}, \qquad n, r = 1, \ldots, N_d \tag{1.7}$$

which means the modes are also **K**-orthogonal. Using Equation (1.3) in Equation (1.1) and premultiplying by $\boldsymbol{\varphi}_n^T$ we obtain

$$\sum_{r=1}^{N_d} \boldsymbol{\varphi}_n^T \mathbf{M} \boldsymbol{\varphi}_r \ddot{q}_r + \sum_{r=1}^{N_d} \boldsymbol{\varphi}_n^T \mathbf{C} \boldsymbol{\varphi}_r \dot{q}_r + \sum_{r=1}^{N_d} \boldsymbol{\varphi}_n^T \mathbf{K} \boldsymbol{\varphi}_r q_r = \boldsymbol{\varphi}_n^T \mathbf{p} \tag{1.8}$$

We now make use of **M**-orthonormality of the modes and the classical damping Equation (1.2) to simplify Equation (1.8) to

$$\ddot{q}_n + 2\zeta_n \omega_n \dot{q}_n + \omega_n^2 q_n = \boldsymbol{\varphi}_n^T \mathbf{p} \tag{1.9}$$

where $\zeta_n = \frac{a_M}{2} \frac{1}{\omega_n} + \frac{a_K}{2} \omega_n$ is the damping ratio of the n-th mode (Chopra 1995).

According to Equation (1.9), the response of a structure under a dynamic load depends on its natural frequencies ω_n and damping ratios ζ_n.

4. MAXIMIZING EIGENFREQUENCIES IN FREE VIBRATION

As seen in the previous section, controlling the response of structures can involve eigenfrequency optimization. In this section we address the problem of maximizing the fundamental frequency of a structure in free vibration. This problem was initially addressed by Díaz and Kikuchi (1992) using the homogenization method. Here, we formulate the problem using the SIMP approach. This formulation can be simply extended to maximizing (or minimizing) any combination of natural frequencies. A practically useful example of such extensions will be briefly addressed in section 6. It is worth noting that maximizing fundamental frequency results in structures with a reasonable stiffness against static loads in general (Bendsøe and Sigmund 2003).

Damping effects are ignored and linear elastic material behavior is assumed in this section. Also all material parameters are taken as deterministic quantities. Random variability of material strength parameters can significantly affect the ductility and energy absorption capacities of structures subjected to seismic loading (Kuwamura and Kato 1989, Elnashai and Chryssanthopoulos 1991). Uncertainties of variables can be considered in structural optimization by integrating Reliability Analysis (see e.g. Kharmanda et al. 2004 and Papadrakakis et al. 2005) or through Robust Optimization (see e.g. Beyer and Sendhoff 2007).

Using the finite element discretization and the SIMP approach we introduce the following material interpolation scheme to express the Young's modulus E_e of element e in terms of its relative density x_e as

$$E_e(x_e) = x_e^p \bar{E} \tag{1.10}$$

where $\bar{E}$ is the Young's modulus of the base isotropic material. The power $p > 1$ is known as the penalty factor and is introduced to push the solutions towards a solid-void topology. A typical value for the penalty factor is $p = 3$ (Bendsøe and Sigmund 1999). The relative densities are changing in the range $0 \leq x_e \leq 1$ in which $x_e = 1$ represents solids and $x_e = 0$ represents void areas. In order to avoid singularities in the stiffness matrix of the system, Equation (1.10) may be replaced by

$$E_e(x_e) = \underline{E} + x_e^p (\bar{E} - \underline{E}) \tag{1.11}$$

in which $\underline{E}$ is a small elastic modulus assigned to voids. Based on Equation (1.10), the (local

level) stiffness matrix of the element e can be expressed as

$$\mathbf{K}_e(x_e) = \underline{\mathbf{K}}_e + x_e^p \left(\bar{\mathbf{K}}_e - \underline{\mathbf{K}}_e\right) \tag{1.12}$$

in which $\bar{\mathbf{K}}_e$ and $\underline{\mathbf{K}}_e$ are the stiffness matrices of the element e when it is made of the base material and void (in its solid and void states) respectively. Similarly for the density and the mass matrix of the element e we can write

$$\rho_e(x_e) = x_e \bar{\rho} \tag{1.13}$$

and

$$\mathbf{M}_e(x_e) = x_e \bar{\mathbf{M}}_e \tag{1.14}$$

Where $\bar{\rho}$ is the density of the base material and $\bar{\mathbf{M}}_e$ is the mass matrix of the element e in its solid state.

Using these material interpolation schemes one can change element e from solid to void and backwards by changing the value of x_e. Thus by choosing x_e-s as design variables, one can produce different topologies without altering the finite element mesh.

We can now formulate the optimization problem. The fundamental frequency optimization problem can be stated as finding the best topology of a structure to maximize its fundamental frequency given a fixed amount of material. The problem can thus be formulated as

$$\begin{aligned} \max_{x_1,x_2,\ldots,x_N} \quad & \left\{\lambda_1 = \min_{j=1,2,\ldots,N_d} \lambda_j\right\} \\ \text{such that} \quad & \mathbf{K}\boldsymbol{\varphi}_j = \lambda_j \mathbf{M}\boldsymbol{\varphi}_j, \qquad j = 1,2,\ldots,N_d \\ & \sum_{e=1}^{N} x_e v_e \le \bar{v} \\ & 0 \le x_e \le 1, \qquad e = 1,2,\ldots,N \end{aligned} \tag{1.15}$$

where $\lambda_j = \omega_j^2, j = 1,\ldots,N_d$ and N is the number of elements. The second constraint restricts the volume of the design to an upper limit denoted by $\bar{v}$. In this statement v_e is the volume of the element e.

4.1. Sensitivity Analysis

Solving Problem (1.15) requires finding the sensitivities of λ_1 with respect to design variables x_e. Differentiating $\mathbf{K}\boldsymbol{\varphi}_j = \lambda_j \mathbf{M}\boldsymbol{\varphi}_j$ we can write

$$\frac{\partial \mathbf{K}}{\partial x_e}\boldsymbol{\varphi}_j + \mathbf{K}\frac{\partial \boldsymbol{\varphi}_j}{\partial x_e} = \frac{\partial \lambda_j}{\partial x_e}\mathbf{M}\boldsymbol{\varphi}_j + \lambda_j \frac{\partial \mathbf{M}}{\partial x_e}\boldsymbol{\varphi}_j + \lambda_j \mathbf{M}\frac{\partial \boldsymbol{\varphi}_j}{\partial x_e} \tag{1.16}$$

Premultiplying by $\boldsymbol{\varphi}_j^T$ and rearranging the terms we obtain

$$\boldsymbol{\varphi}_j^T \left(\frac{\partial \mathbf{K}}{\partial x_e} - \lambda_j \frac{\partial \mathbf{M}}{\partial x_e}\right)\boldsymbol{\varphi}_j = \frac{\partial \lambda_j}{\partial x_e}\boldsymbol{\varphi}_j^T \mathbf{M}\boldsymbol{\varphi}_j - \boldsymbol{\varphi}_j^T \left(\mathbf{K} - \lambda_j \mathbf{M}\right)\frac{\partial \boldsymbol{\varphi}_j}{\partial x_e} \tag{1.17}$$

Using the symmetry of $\mathbf{K}$ and $\mathbf{M}$, we can readily conclude that

$$\boldsymbol{\varphi}_j^T \left(\mathbf{K} - \lambda_j \mathbf{M}\right) = \left[\left(\mathbf{K} - \lambda_j \mathbf{M}\right)\boldsymbol{\varphi}_j\right]^T = 0\,.$$

We also use Equation (1.6) in Equation (1.17) to finally express the sensitivities as

$$\frac{\partial \lambda_j}{\partial x_e} = \boldsymbol{\varphi}_j^T \left(\frac{\partial \mathbf{K}}{\partial x_e} - \lambda_j \frac{\partial \mathbf{M}}{\partial x_e}\right)\boldsymbol{\varphi}_j \tag{1.18}$$

The stiffness and mass derivatives in Equation (1.18) can be calculated using Eqs. (1.12) and (1.14).

4.2. Solution Method

Having the sensitivities in Equation (1.18), the optimization problem (1.15) can be solved using

suitable gradient-based techniques. Noting that the number of design variables (number of elements) can be very large, one should adopt a solution method capable of solving large-scale problems. The method of moving asymptotes (MMA) proposed by Svanberg (1987) is a well-known solution method used in topology optimization problems. Another common approach is using optimality criteria (OC) based algorithms. In the following, after deriving the optimality criteria for the optimization problem (1.15), we propose a heuristic iterative fixed-point algorithm to solve the optimization problem based on the optimality criteria.

The eigenvalue equation, $\mathbf{K}\boldsymbol{\varphi}_j = \lambda_j \mathbf{M}\boldsymbol{\varphi}_j$ can be satisfied separately using finite element analysis. Excluding this equation, the Lagrangian of Problem (1.15) takes the form

$$\mathcal{L} = \lambda_1 + \Gamma\left(\overline{v} - \sum_{e=1}^{N} x_e v_e\right) + \sum_{e=1}^{N}\left[\overline{\gamma}_e\left(1 - x_e\right) + \underline{\gamma}_e x_e\right] \tag{1.19}$$

where Γ, $\overline{\gamma}_e$ and $\underline{\gamma}_e$ are Lagrange multipliers. Using Karush-Kuhn-Tucker results (Karush 1939; Kuhn and Tucker 1951), the necessary optimality conditions for Problem (1.15) can be expressed as follows

$$\begin{aligned}
&\frac{\partial \mathcal{L}}{\partial x_e} = \frac{\partial \lambda_1}{\partial x_e} - \Gamma v_e - \overline{\gamma}_e + \underline{\gamma}_e = 0 \\
&\Gamma\left(\overline{v} - \sum_{e=1}^{N} x_e v_e\right) = 0; \qquad \overline{v} - \sum_{e=1}^{N} x_e v_e \geq 0; \qquad \Gamma \geq 0 \\
&\overline{\gamma}_e\left(1 - x_e\right) = 0; \qquad 1 - x_e \geq 0; \qquad \overline{\gamma}_e \geq 0, \qquad e = 1,\ldots N \\
&\underline{\gamma}_e x_e = 0; \qquad\qquad x_e \geq 0; \qquad\qquad \underline{\gamma}_e \geq 0, \qquad e = 1,\ldots N
\end{aligned} \tag{1.20}$$

If we define $\gamma_e = \overline{\gamma}_e - \underline{\gamma}_e$ and use it in Equation (1.20), we can rewrite the optimality criteria as

$$\begin{aligned}
&D_e = \frac{\partial \lambda_1}{\partial x_e} - \Gamma v_e = \gamma_e \\
&\Gamma\left(\overline{v} - \sum_{e=1}^{N} x_e v_e\right) = 0; \quad \overline{v} - \sum_{e=1}^{N} x_e v_e \geq 0; \quad \Gamma \geq 0 \\
&\qquad x_e = 0 \qquad\Rightarrow\quad \gamma_e \leq 0 \\
&\qquad 0 < x_e < 1 \qquad\Rightarrow\quad \gamma_e = 0 \\
&\qquad x_e = 1 \qquad\Rightarrow\quad \gamma_e \geq 0 \\
&\qquad\qquad e = 1,\ldots,N
\end{aligned} \tag{1.21}$$

To increase the fundamental frequency, we add a vector of increments $\Delta\mathbf{x} = (\Delta x_1, \Delta x_2,\ldots, \Delta x_N)^T$ to the design variables $\mathbf{x} = (x_1, x_2,\ldots, x_N)^T$. The subsequent change in the fundamental frequency and the design volume can then be evaluated as

$$\Delta\lambda_1 = \left(\nabla\lambda_1\right)^T \Delta\mathbf{x} \tag{1.22}$$

$$\Delta v = \mathbf{v}^T \Delta\mathbf{x} \tag{1.23}$$

where $\nabla\lambda_1 = \left(\frac{\partial\lambda_1}{\partial x_1}, \frac{\partial\lambda_1}{\partial x_2}, \ldots, \frac{\partial\lambda_1}{\partial x_N}\right)^T$ is the gradient vector of λ_1 and $\mathbf{v} = (v_1, v_2, \ldots, v_N)^T$.

Let us now define the increments of design variables as

$$\Delta\mathbf{x} = \mathbf{D} = \nabla\lambda_1 - \Gamma\mathbf{v} \tag{1.24}$$

If the volume constraint is inactive, we will have $\Gamma = 0$ and thus $\Delta\mathbf{x} = \nabla\lambda_1$ which results in $\Delta\lambda_1 = \left(\nabla\lambda_1\right)^T \nabla\lambda_1 \geq 0$ after substituting in Equation (1.22).

If the volume constraint is active, on the other hand, we will have

$$\Delta v = \mathbf{v}^T \Delta\mathbf{x} = 0 \tag{1.25}$$

Using Equation (1.24) in Equation (1.25) and solving for Γ we obtain

$$\Gamma = \frac{\mathbf{v}^T \nabla \lambda_1}{\mathbf{v}^T \mathbf{v}} \tag{1.26}$$

If the boxing conditions are all inactive, i.e. if $0 < x_e < 1$, we can use Equation (1.26) in Equation (1.24) and then Equation (1.24) in Equation (1.22) to write

$$\Delta\lambda_1 = \left(\nabla\lambda_1\right)^T \left(\nabla\lambda_1 - \frac{\mathbf{v}^T \nabla\lambda_1 \mathbf{v}}{\mathbf{v}^T \mathbf{v}}\right) \tag{1.27}$$

It can be easily verified that the right hand side of Equation (1.27) is a form of Cauchy–Bunyakovsky–Schwarz inequality and thus $\Delta\lambda_1 \geq 0$.

Based on this discussion, we propose the following update scheme to solve Problem (1.15)

$$\mathbf{x}_{(k+1)} = \max\left\{0, \left(\mathbf{x}_{(k)} - \eta\right), \min\left\{1, \left(\mathbf{x}_{(k)} + \eta\right), \left(\mathbf{x}_{(k)} + \eta \mathbf{D}_{(k)} \left|\mathbf{D}_{(k)}\right|^{\frac{1-p}{p}}\right)\right\}\right\} \tag{1.28}$$

Here the subscripts denote the iteration number and η is a tuning parameter defining the move limit. The vector $\mathbf{D}$ is defined in Equation (1.24). Note that p used here is the previously defined penalty power for stiffness. The value of the Lagrange multiplier Γ can be calculated using bisection method in an inner loop. In finding Γ, one should note that $\partial v / \partial \Gamma < 0$.

Note that the same algorithm can be used to maximize any of the natural frequencies. To maximize the kth eigenvalue, for example, one needs to replace λ_1 and $\boldsymbol{\varphi}_1$ by λ_k and $\boldsymbol{\varphi}_k$ respectively.

4.3. Numerical Instabilities

Most of the material distribution techniques, including homogenization, SIMP and BESO methods, are known to be prone to three major numerical instabilities, namely checkerboard problem, mesh dependency, and local minima (Sigmund and Petersson 1998). Checkerboard problem refers to the formation of alternating solid and void elements in a checkerboard-like pattern resulting in artificially high stiffness. Mesh dependency refers to obtaining different optimal topologies for the same problem using different mesh sizes. Local minima refers to the problem of obtaining different optimal topologies using the same mesh but different algorithmic parameters and/or initial design.

One of the simplest yet effective approaches to overcome checkerboard and mesh dependence problems is filtering sensitivities (Sigmund and Petersson 1998). In this approach the calculated sensitivities are replaced by filtered sensitivities which are calculated as a weighted average of the sensitivities of the neighboring elements. A simple linear filter takes the form

$$\widehat{\frac{\partial \lambda}{\partial x_i}} = \frac{\sum_{e=1}^{N} x_j \frac{\partial \lambda}{\partial x_j} w_{ij}}{x_i \sum_{j=1}^{N} w_{ij}} \tag{1.29}$$

in which $w_{ij} = \max\{0, R - d_{ij}\}$. R is known as the filtering radius and d_{ij} denotes the distance between the centers of the elements i and j. The filtering scheme (1.29) can be activated by choosing the filtering radius R bigger than the size of elements h. This can eliminate the checkerboard problem.

In this scheme, the filtering radius R imposes a local minimum length scale to the solutions. More precisely, using this sensitivity filter, the width of bars appearing in the resulting topologies could not be smaller than $2R$. This property is useful in achieving mesh independency. By defining R as a ratio of the actual length of the design domain, the mesh dependence problem can be rectified.

Unlike the first two types of numerical instabilities, the local minima problem is mostly due to the use of gradient-based optimization algorithm which can be trapped in local minima of usually non-convex objective functions. On the other

hand, the extremely large size of the problems in topology optimization is a great barrier in using non-gradient-based optimization techniques such as Genetic Algorithm (GA) and Neural Networks. The *continuation* method is a simple approach used and suggested by many researchers to overcome this problem in gradient-based optimization methods (Sigmund and Petersson 1998). In this approach, one would start solving the problem in a more relaxed form and gradually apply restrictions. For example, one can start the solution considering no penalty factor (p = 1) and gradually increase p upon convergence of the solution.

Apart from these three problems – which are common in all types of topology optimization problems – some numerical artifacts are unique to eigenvalue problems. The 'artificial modes' problem comes under this category. These are localized modes appearing in regions with relatively high mass to stiffness ratio. Pedersen (2000) points that due to the interpolation schemes for stiffness and mass (Eqs. (1.12) and (1.14) respectively), the mass to stiffness ratio rises steeply for small values of x which ultimately results in localized modes. To overcome this problem, a modification in the stiffness interpolation scheme is suggested by Pedersen (2000) to limit the mass to stiffness ratio in low density areas (typically $x < 0.1$). Following the same principle, Du and Olhoff (2007) proposed a different approach by modifying the mass interpolation scheme. The latter approach is adopted here. To this end, we replace the original mass interpolation scheme, Equation (1.14), by

$$\mathbf{M}_e(x_e) = \begin{cases} x_e \bar{\mathbf{M}}_e, & x_e > 0.1 \\ 10^{q-1} x_e^q \bar{\mathbf{M}}_e, & x_e \leq 0.1 \end{cases} \qquad (1.30)$$

with $q = 2p$. This ensures that the mass to stiffness ratio cannot exceed 10^{p-1}.

4.4. Flowchart and Numerical Examples

A flowchart of the proposed solution algorithm is depicted in Figure 2. The solution starts from an initial guess design. A uniform distribution of material defined as $x_e = \bar{v} / v_t$, $e = 1, \ldots, N$ with v_t denoting the total volume of the design domain is usually used as an initial design. The main loop starts by analyzing the current design using finite element analysis. Based on FE results, the sensitivities are calculated using Equation (1.18). The sensitivities are then filtered using Equation (1.29). The updated variables are calculated in an inner loop. In the inner loop, starting with a positive value for the Lagrange multiplier Γ, the updated variables are calculated using Equation (1.28). The volume of this new design is checked and the new value of Γ is adjusted using the bisection approach. The inner loop continues until the value of Γ converges. The updated design is then replaces the old one and the procedure is repeated until a convergence criterion is satisfied.

The convergence criterion used here is defined as

$$\frac{\left| \sum_{i=k-l+1}^{k} \lambda_{(i)} - \sum_{i=k-l}^{k-1} \lambda_{(i)} \right|}{\sum_{i=k-l+1}^{k} \lambda_{(i)} + \sum_{i=k-l}^{k-1} \lambda_{(i)}} \leq \varepsilon \qquad (1.31)$$

where $\lambda_{(i)}$ is the value of the objective function at the i-th iteration and k denotes the last iteration. This condition compares the value of the objective function in the last and second last l iterations and assumes convergence is achieved when the relative error is smaller than a predefined tolerance $0 < \varepsilon \ll 1$. In all examples reported here l = 5 and ε = 0.001 were used.

Figure 2. The flowchart of the proposed solution algorithm

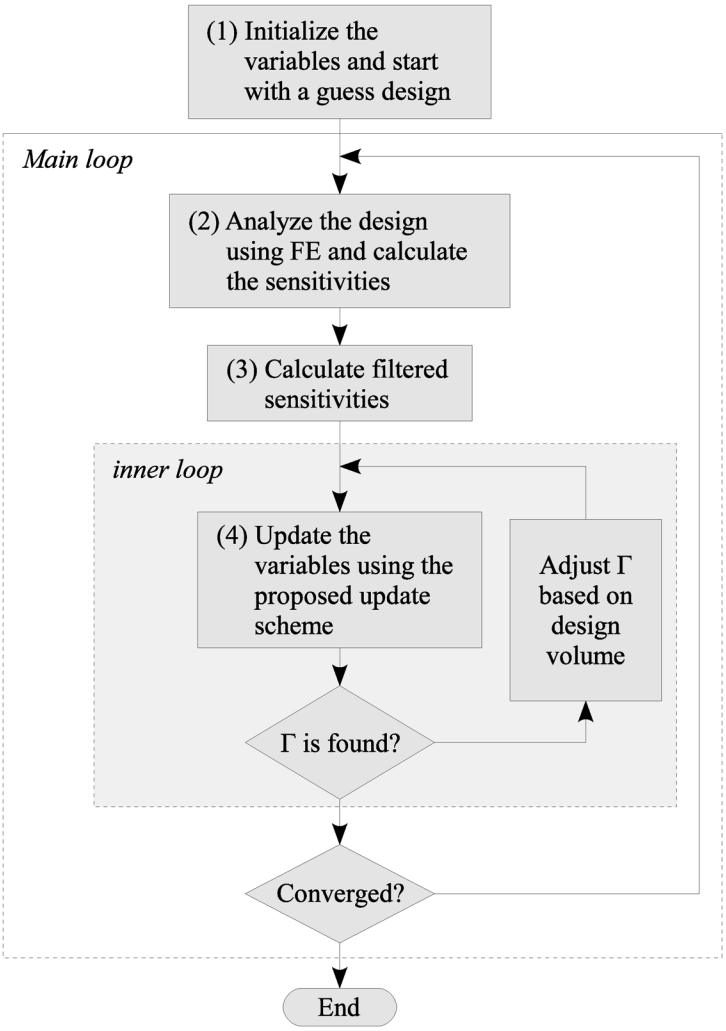

Example 1: Reinforcement of a Planar Frame

As the first example we consider a frame in plane stress. The maximum volume of used material should be limited to half of the volume of the whole frame ($\overline{v} / v_t = 50\%$). The initial design is depicted in Figure 3 (leftmost). The outer frame is fixed to be solid and is non-designable. Note that if we do not consider the non-designable outer frame, the optimization program will obviously shorten the frame.

The 3×12m domain is descretized using a 30×120 mesh of 4 node square bi-linear elements. A consistent mass matrix formulation has been used (see e.g. Zienkiewicz et al. 2005). The stiffness and density of the base material are assumed as $\overline{E} = 2 \times 10^5$ MPa and $\rho = 8000\,\mathrm{kg/m^3}$ respectively. A penalty power of $p = 4$, a filtering radius of $R = 30\mathrm{cm} = 3h$, and move limit of $\eta = 0.2$ have been used. The ratio between the stiffness of solid and void areas is selected as $\overline{E} : \underline{E} = 10^9$.

The obtained topologies at different iterations are shown in Figure 3.

Figure 3. The initial design and topologies of the first example at different iteration numbers

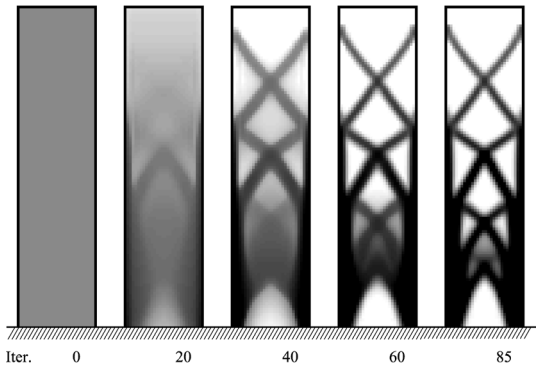

Figure 4 shows the values of the fundamental frequency and the first eigenmode. The fundamental frequency has increased from 60.4 rad/s in initial design to 154.1 rad/s after 85 iterations showing 155% increase. Note that the values of the fundamental frequency also depend on the penalty factor. If we analyze these designs with $p = 1$, the initial and final eigenfrequencies will change to 105.2 rad/s and 174.0 rad/s respectively.

5. MULTIPLE EIGENFREQUENCIES

By steadily increasing (or decreasing) an eigenfrequency, it is possible that its value reaches adjacent eigenfrequencies resulting in multiple eigenfrequencies. The problem of multiple eigenvalues in structural optimization was first addressed by Olhoff and Rasmussen (1977). It is shown by Haug and Rousselet (1980) that the multiple eigenvalues are not differentiable in the Fréchet sense and can only be expected to be Gâteaux (directionally) differentiable. This finding rules out the validity of sensitivities calculated by Equation (1.18) in case of multiple eigenfrequencies. Ignoring this fact in topology optimization will result in oscillation of

Figure 4. Evolution history of the fundamental frequency (a) and the first eigenmode of the optimal design (b) in example 1

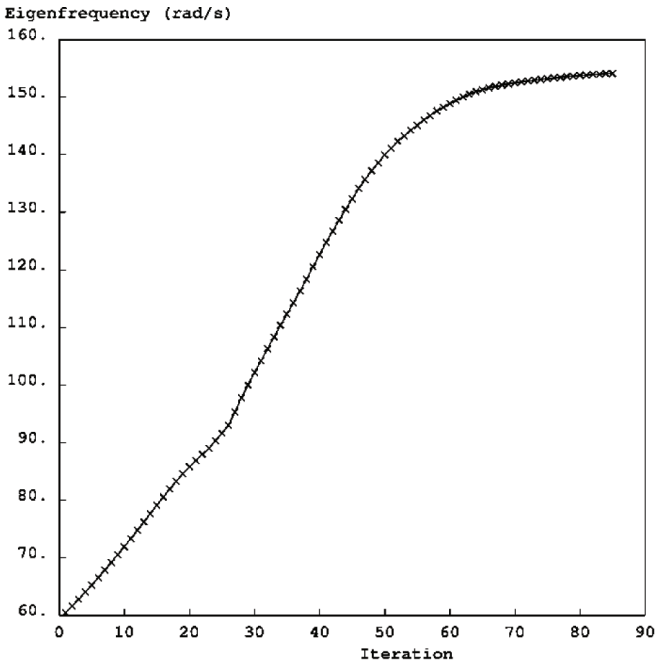

(a)

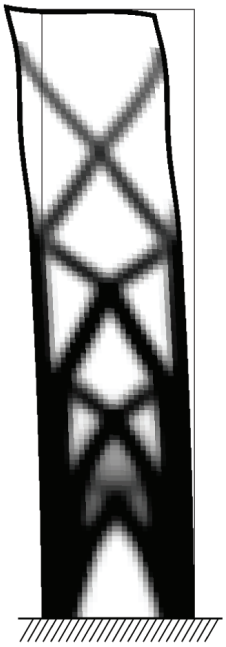

(b)

the objective function and suboptimal solutions as shown in the following example.

Example 2: Clamped-Clamped Beam

Consider the problem of maximization of the fundamental frequency of a clamped-clamped beam with volume fraction of 50% and material properties similar to example 1. All algorithmic parameters are similar to example 1. The structure has been discretized into 30×240 identical 4-node bi-linear square elements. The initial and the final solutions and the evolution of the first three eigenfrequencies are shown in Figure 5.

It can be seen that after 29 iterations, the first two eigenfrequencies coalesce. Using the single modal sensitivities of Equation (1.18), decreases the objective function instead of increasing it. This produces oscillation after the point of coalesce and the algorithm converges at a suboptimal solution (Figure 5b).

5.1. Simple Approaches to Avoid Multiple Eigenfrequencies

A number of simple approaches can be used to avoid multiple eigenfrequencies. Kosaka and Swan (1999) proposed a symmetry reduction approach in which a symmetry condition is imposed on the design variables to ensure a symmetric solution. In their paper, Kosaka and Swan (1999) noted that in a symmetric structure, the multiple

Figure 5. Example 2 without treatment: initial design (a), final solution (b), and evolution of the eigenfrequencies (c)

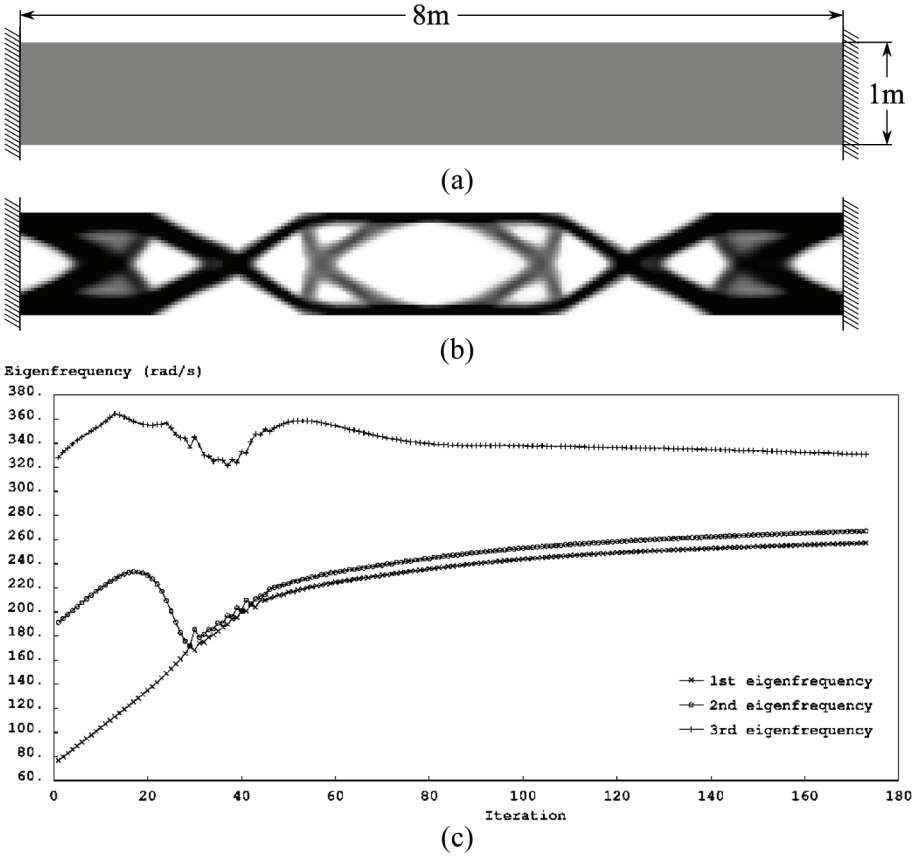

eigenvalues are differentiable (in the Fréchet sense). Note that in this approach the symmetry reduction is not applied in the analysis and the analysis is based on the full structure. Using symmetry reduced structure for analysis cannot be validated in eigenfrequency optimization since the eigenmodes are not necessarily symmetric even for a symmetric structure.

Another approach to avoid repeated eigenfrequencies is to add an extra condition to the optimization problem ensuring that the eigenfrequencies are distant from each other. For example one may reformulate problem (1.15) as follows (Bendsøe and Sigmund 2003).

$$\begin{aligned} \max_{x_1,x_2,\ldots,x_N} \quad & \beta \\ \text{such that} \quad & \alpha^j \lambda_j \geq \beta, \qquad j = 1,2,\ldots,N_d \\ & \mathbf{K}\boldsymbol{\varphi}_j = \lambda_j \mathbf{M}\boldsymbol{\varphi}_j, \qquad j = 1,2,\ldots,N_d \\ & \sum_{e=1}^{N} x_e v_e \leq \overline{v} \\ & 0 \leq x_e \leq 1, \qquad e = 1,2,\ldots,N \end{aligned} \tag{1.32}$$

with $\alpha < 1$, for example $\alpha = 0.95$. This formulation is known as *bound formulation*. Note that with $\alpha = 1$, Problem (1.32) is equivalent to Problem (1.15).

It is also possible to turn around the multiple eigenvalue problem by including adjacent eigenfrequencies in the objective function. For example Yang et al. (1999b) used the arithmetic mean of the eigenvalues as the objective function when

Figure 6. Solving example 2, using mean eigenfrequency as objective function: final solution (a) and evolution of the objective function and the first three eigenfrequencies (b)

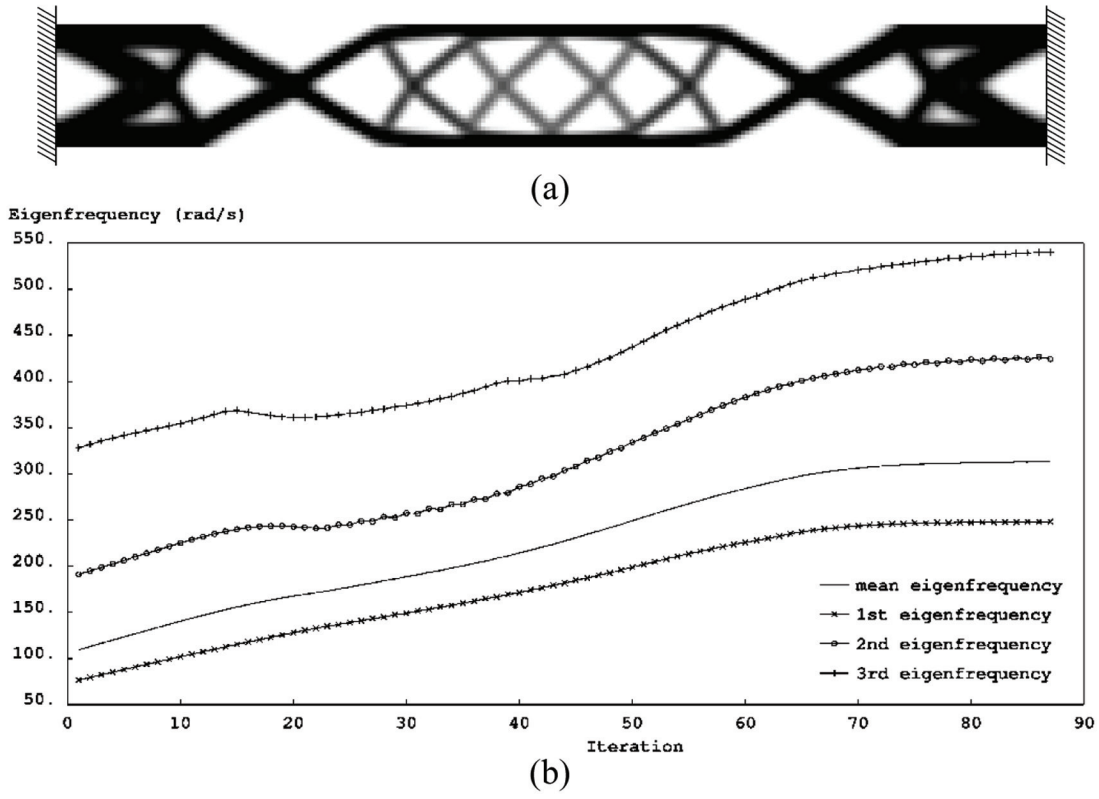

they fell within a small distance from each other. A more generalized mean eigenvalue objective function has been considered by Ma et al. (1995). For example considering the harmonic mean of the first two eigenvalues, we can define the following objective function

$$\lambda^* = 2\left(\lambda_1^{-1} + \lambda_2^{-1}\right)^{-1} \tag{1.33}$$

Using this objective function in example 2 results in a smooth increase for the first two eigenvalues. Figure 6 shows the final solution and the evolution history of the first three eigenvalues considering the objective function defined in Equation (1.33) in example 2.

5.2. Sensitivity Analysis of Multiple Eigenvalues

It is also possible to solve the multimodal eigenfrequency optimization problems directly. Using a perturbation technique, Bratus and Seyranian (1983) calculated the sensitivities of multiple eigenvalues. Here we follow Seyranian et al. (1994) and Lund (1994) to present the sensitivity analysis of multiple eigenfrequencies.

Assume an m-fold multiple eigenvalue

$$\lambda_j = \tilde{\lambda}, \quad j = 1,\ldots,m \tag{1.34}$$

Due to multiplicity, any linear combination of the corresponding eigenvectors will satisfy the main eigenvalue problem $\mathbf{K}\boldsymbol{\varphi}_j = \lambda_j \mathbf{M}\boldsymbol{\varphi}_j$. Now assume the following linear combination

$$\tilde{\boldsymbol{\varphi}}_j = \sum_{k=1}^{m} \alpha_{jk}\boldsymbol{\varphi}_k, \quad j = 1,\ldots,m \tag{1.35}$$

where the coefficients α_{jk} are unknown. If we apply a perturbation ε to the i-th optimization variable the vector of design variables changes to $\mathbf{x} + \varepsilon\Delta\mathbf{x}_i$ where $\Delta\mathbf{x}_i$ denotes a vector of size N, all of its components being zero except for its i-th component which is 1.

Due to this perturbation, the stiffness and mass matrices will change to

$$\begin{aligned} \mathbf{K}(\mathbf{x} + \varepsilon\Delta\mathbf{x}_i) &= \mathbf{K} + \varepsilon\frac{\partial\mathbf{K}}{\partial x_i} + o(\varepsilon), \\ \mathbf{M}(\mathbf{x} + \varepsilon\Delta\mathbf{x}_i) &= \mathbf{M} + \varepsilon\frac{\partial\mathbf{M}}{\partial x_i} + o(\varepsilon) \end{aligned} \tag{1.36}$$

and the eigenvalues and the eigenvectors will change to

$$\lambda_j(\mathbf{x} + \varepsilon\Delta\mathbf{x}_i) = \tilde{\lambda} + \varepsilon\mu_j + o(\varepsilon), \quad j = 1,\ldots,m \tag{1.37}$$

$$\boldsymbol{\varphi}_j(\mathbf{x} + \varepsilon\Delta\mathbf{x}_i) = \tilde{\boldsymbol{\varphi}}_j + \varepsilon\boldsymbol{\nu}_j + o(\varepsilon), \quad j = 1,\ldots,m \tag{1.38}$$

where μ_j and $\boldsymbol{\nu}_j$ are the unknown sensitivities of the multiple eigenvalues and eigenvectors respectively. $o(\varepsilon)$ indicates higher order terms. Note that $\mu_j \equiv \mu_j(\mathbf{x}, \Delta\mathbf{x}_i)$ and $\boldsymbol{\nu}_j \equiv \boldsymbol{\nu}_j(\mathbf{x}, \Delta\mathbf{x}_i)$, i.e. the sensitivities depend on $\Delta\mathbf{x}_i$.

Using the perturbed values of Eqs. (1.36), (1.37), and (1.38) in the main eigenvalue problem, after ignoring the higher terms, one obtains

$$\left(\frac{\partial\mathbf{K}}{\partial x_i} - \tilde{\lambda}\frac{\partial\mathbf{M}}{\partial x_i}\right)\tilde{\boldsymbol{\varphi}}_j + \left(\mathbf{K} - \tilde{\lambda}\mathbf{M}\right)\boldsymbol{\nu}_j = \mu_j\mathbf{M}\tilde{\boldsymbol{\varphi}}_j \tag{1.39}$$

Premultiplying Equation (1.39) by $\boldsymbol{\varphi}_s^T$, $s = 1,\ldots,m$, the second term in the left-hand side will cancel out and one obtains the following m equations

$$\boldsymbol{\varphi}_s^T\left(\frac{\partial\mathbf{K}}{\partial x_i} - \tilde{\lambda}\frac{\partial\mathbf{M}}{\partial x_i}\right)\tilde{\boldsymbol{\varphi}}_j = \mu_j\boldsymbol{\varphi}_s^T\mathbf{M}\tilde{\boldsymbol{\varphi}}_j, \quad s = 1,\ldots,m \tag{1.40}$$

We now substitute Equation (1.35) in Equation (1.40) and use Equation (1.6) to write

$$\sum_{k=1}^{m} \alpha_{jk} \left[\boldsymbol{\varphi}_s^T \left(\frac{\partial \mathbf{K}}{\partial x_i} - \tilde{\lambda} \frac{\partial \mathbf{M}}{\partial x_i} \right) \boldsymbol{\varphi}_k - \mu_j \delta_{sk} \right] = 0, \quad s = 1, \ldots, m \tag{1.41}$$

This linear system can be solved to calculate the coefficients α_{jk}. A non-trivial solution only exists if

$$\det \left[\boldsymbol{\varphi}_s^T \left(\frac{\partial \mathbf{K}}{\partial x_i} - \tilde{\lambda} \frac{\partial \mathbf{M}}{\partial x_i} \right) \boldsymbol{\varphi}_k - \mu_j \delta_{sk} \right] = 0, \quad s,k = 1, \ldots, m \tag{1.42}$$

This subeigenvalue problem can be solved to calculate the sensitivities $\mu_j, j = 1,\ldots,m$ due to the increment of the i-th optimization variable.

If the vector of design variables undergo an increment of the form $\varepsilon\mathbf{e}$ with $\mathbf{e} = (\Delta x_1, \Delta x_2, \ldots, \Delta x_N)^T$ and $\|\mathbf{e}\| = 1$, one can easily generalize Equation (1.42) to

$$\det \left[\mathbf{f}_{sk}^T \mathbf{e} - \mu \delta_{sk} \right] = 0, \quad s,k = 1, \ldots, m \tag{1.43}$$

where

$$\mathbf{f}_{sk}^T = \left(\boldsymbol{\varphi}_s^T \left(\frac{\partial \mathbf{K}}{\partial x_1} - \tilde{\lambda} \frac{\partial \mathbf{M}}{\partial x_1} \right) \boldsymbol{\varphi}_k, \boldsymbol{\varphi}_s^T \left(\frac{\partial \mathbf{K}}{\partial x_2} - \tilde{\lambda} \frac{\partial \mathbf{M}}{\partial x_2} \right) \boldsymbol{\varphi}_k, \ldots, \boldsymbol{\varphi}_s^T \left(\frac{\partial \mathbf{K}}{\partial x_N} - \tilde{\lambda} \frac{\partial \mathbf{M}}{\partial x_N} \right) \boldsymbol{\varphi}_k \right)^T, \quad s,k = 1, \ldots, m \tag{1.44}$$

are known as the generalized gradient vectors (Seyranian et al. 1994). Note that $\mathbf{f}_{sk}$ are vectors of length N, thus $\mathbf{f}_{sk}^T \mathbf{e}$ are scalars. Also note that due to symmetry of the stiffness and mass matrices $\mathbf{f}_{sk} = \mathbf{f}_{ks}$.

The solutions of subeigenvalue problem of Equation (1.43) are the sensitivities of the multiple eigenvalues. This equation was initially introduced by Bratus and Seyranian (1983).

5.3. Solution Algorithm

Assume that $\boldsymbol{\Phi}$ is an $N_d \times m$ matrix whose columns are the eigenvectors $\boldsymbol{\varphi}_1, \ldots, \boldsymbol{\varphi}_m$. Also consider the vector $\mathbf{d} = (d_1, d_2, \ldots, d_N)^T$ defined as

$$d_e = \frac{\partial \mathbf{K}}{\partial x_e} - \tilde{\lambda} \frac{\partial \mathbf{M}}{\partial x_e}, \quad e = 1, \ldots, N \tag{1.45}$$

Then the subeigenvalue problem of Equation (1.43) can be stated in the following matrix form

$$\mathbf{A} - \mu \mathbf{I} = 0 \tag{1.46}$$

where $\mathbf{A} = \boldsymbol{\Phi}^T \boldsymbol{\Phi} \mathbf{d}^T \mathbf{e}$ is a symmetric $m \times m$ matrix and $\mathbf{I}_{m \times m}$ is the unity matrix.

Following Cox and Overton (1992) and Overton (1992), the necessary optimality conditions to solve problem (1.15) is that there exists an $m \times m$ symmetric positive semidefinite matrix $\boldsymbol{\Lambda}$ with trace($\boldsymbol{\Lambda}$) = 1 such that

$$\begin{gathered} \tilde{D}_e = \boldsymbol{\Lambda} : \left(\boldsymbol{\Phi}^T d_e \boldsymbol{\Phi} \right) - \Gamma v_e = \gamma_e \\ \Gamma \left(\overline{v} - \sum_{e=1}^{N} x_e v_e \right) = 0; \quad \overline{v} - \sum_{e=1}^{N} x_e v_e \geq 0; \quad \Gamma \geq 0 \\ \begin{aligned} x_e = 0 \quad &\Rightarrow \quad \gamma_e \leq 0 \\ 0 < x_e < 1 \quad &\Rightarrow \quad \gamma_e = 0 \\ x_e = 1 \quad &\Rightarrow \quad \gamma_e \geq 0 \end{aligned} \\ e = 1, \ldots, N \end{gathered} \tag{1.47}$$

where the Frobenius matrix inner product is defined as $\mathbf{A}:\mathbf{B}$ = trace($\mathbf{A}^T\mathbf{B}$).

The proof of optimality conditions in (1.47) will not be presented here. Enthusiast reader is referred to Cox and Overton (1992), Overton (1992), and Seyranian et al. (1994).

Note that for the case of simple eigenvalues (m = 1), one should have $\Lambda = 1$ and optimality conditions in (1.47) reduce to (1.21). Comparing (1.47) with (1.21), one may note that the only difference is that the sensitivities $\partial\lambda/\partial x_e$ in (1.21) have been

replaced by $\mathbf{\Lambda}$:($\mathbf{\Phi}^T d_e \mathbf{\Phi}$) in (1.47). The only issue here is to find a suitable matrix $\mathbf{\Lambda}$.

Similar to Equation (1.24), we consider the following increment vector

$$\Delta x_e = \tilde{D}_e = \mathbf{\Lambda} : \left(\mathbf{\Phi}^T d_e \mathbf{\Phi}\right) - \Gamma v_e, \quad e = 1,\ldots,N \tag{1.48}$$

To illustrate the calculation of $\mathbf{\Lambda}$, we consider the simplest multiple case of $m = 2$. We assume that the two eigenvalues are repeated if

$$\frac{\lambda_2 - \lambda_1}{\lambda_1} \leq \delta \tag{1.49}$$

with δ being a small positive tolerance. In this case we have

$$\mathbf{\Phi} = \left(\boldsymbol{\varphi}_1, \boldsymbol{\varphi}_2\right) \tag{1.50}$$

We also introduce the following positive semidefinite symmetric matrix

$$\mathbf{\Lambda}^* = \begin{pmatrix} \Lambda_{11}^* & \Lambda_{12}^* \\ \Lambda_{12}^* & \Lambda_{22}^* \end{pmatrix} \tag{1.51}$$

based on which we define

$$\mathbf{\Lambda} = \frac{\mathbf{\Lambda}^*}{\text{trace}(\mathbf{\Lambda}^*)} \tag{1.52}$$

to ensure that trace($\mathbf{\Lambda}$) = 1.

Substituting Equation (1.51) in Equation (1.48) and using Eqs. (1.45) and (1.44), we may rewrite Equation (1.48) in the following form

$$\Delta \mathbf{x} = \Lambda_{11}^* \mathbf{f}_{11} + 2\Lambda_{12}^* \mathbf{f}_{12} + \Lambda_{22}^* \mathbf{f}_{22} - \Gamma \mathbf{v} \tag{1.53}$$

The change in the multiple eigenvalues $\Delta\lambda_1$ and $\Delta\lambda_2$ due to $\Delta\mathbf{x}$ can be calculated by solving the following quadratic equation which is emerged from Equation (1.43)

$$\det \begin{pmatrix} \mathbf{f}_{11}^T \Delta \mathbf{x} - \Delta\lambda & \mathbf{f}_{12}^T \Delta \mathbf{x} \\ \mathbf{f}_{12}^T \Delta \mathbf{x} & \mathbf{f}_{22}^T \Delta \mathbf{x} - \Delta\lambda \end{pmatrix} = 0 \tag{1.54}$$

We are interested in finding Λ_{ij}^* such that Equation (1.54) results in two positive eigenvalues $\Delta\lambda_1 > 0$ and $\Delta\lambda_2 > 0$. There are several ways to achieve this. Here we assume the following

$$\Delta\lambda_1 = \mathbf{f}_{11}^T \Delta \mathbf{x} = 1 \tag{1.55}$$

$$\Delta\lambda_2 = \mathbf{f}_{22}^T \Delta \mathbf{x} = 1 - \tfrac{\lambda_2 - \lambda_1}{\lambda_1} \tag{1.56}$$

$$\mathbf{f}_{12}^T \Delta \mathbf{x} = 0 \tag{1.57}$$

Equation (1.57) implies that the matrix in Equation (1.54) is diagonal, hence the eigenvalues are equivalent to the diagonal terms as stated in Eqs. (1.55) and (1.56). In Equation (1.55) we considered an increase of 1 for the lowest eigenvalue. If the two eigenvalues are different, the increase assigned to the second eigenvalue in Equation (1.56) will be slightly lower than 1. This is to reduce the difference between the two repeated eigenvalues.

Substituting Equation (1.53) in Eqs. (1.55) to (1.57), we obtain a set of three equations which can be solved to yield the three unknown coefficients Λ_{11}^*, Λ_{22}^*, and Λ_{22}^*. These equations can be summarized as

$$\begin{bmatrix} \mathbf{f}_{11}^T \mathbf{f}_{11} & \mathbf{f}_{11}^T \mathbf{f}_{22} & \mathbf{f}_{11}^T \mathbf{f}_{12} \\ & \mathbf{f}_{22}^T \mathbf{f}_{22} & \mathbf{f}_{22}^T \mathbf{f}_{12} \\ \text{symm.} & & \mathbf{f}_{12}^T \mathbf{f}_{12} \end{bmatrix} \begin{Bmatrix} \Lambda_{11}^* \\ \Lambda_{22}^* \\ 2\Lambda_{12}^* \end{Bmatrix} = \begin{Bmatrix} 1 + \Gamma \mathbf{f}_{11}^T \mathbf{v} \\ 1 - \frac{\lambda_2 - \lambda_1}{\lambda_1} + \Gamma \mathbf{f}_{22}^T \mathbf{v} \\ \Gamma \mathbf{f}_{12}^T \mathbf{v} \end{Bmatrix} \tag{1.58}$$

By solving Equation (1.58) one finds $\mathbf{\Lambda}^*$ which is used in Equation (1.52) to find $\mathbf{\Lambda}$ and

subsequently $\Delta\mathbf{x}$ from Equation (1.53). Like the single modal case, to find the value of the Lagrange multiplier Γ an inner bisection loop can be used.

Figure 7 shows the final solution and the evolution history of the first three eigenfrequencies of the problem of example 2 using the above approach. It can be seen that the multiple eigenvalues evolve smoothly and a better solution is achieved.

Table 1 compares the final value of the first three eigenfrequencies of example 2 obtained using the three approaches considered here. As expected, using the multiple eigenvalue sensitivities yields the best result.

6. CONTROLLING THE NATURAL FREQUENCIES

In dynamic design of structures one usually requires to control the natural frequencies rather than increasing them. For an objective function defined as a combination of natural frequencies, the optimization problem can usually be addressed by minimal modification of the eigenfrequency maximization problem. Typically one just needs to update the sensitivities. One example of such objective functions was defined in Equation (1.33) and dealt with in the preceding section. Other examples include maximizing the gap between two natural frequencies (see e.g. Du and Olhoff 2007 and Zhao et al. 1997) or designing structures with a specified set of frequencies or eigenmode shapes (see e.g. Xie and Steven 1996, Yang et al. 1999b, Maeda et al. 2006) among others.

A common practical case is where the excitation frequency is known and it is desired to move the natural frequencies as far away as possible from the excitation frequency. A suitable objective function can be defined as

Figure 7. Solving example 2, using multiple eigenvalue sensitivities: final solution (a) and evolution of the first three eigenfrequencies (b)

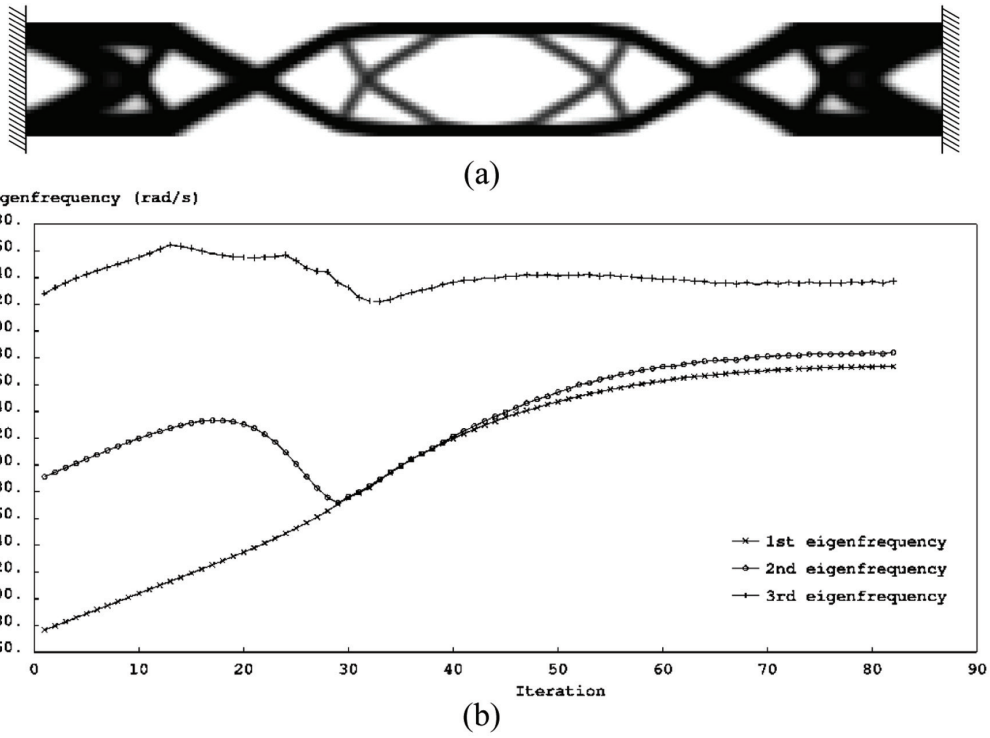

$$f = \sum_{j \in J} \left| \omega_j^2 - \Omega^2 \right| \tag{1.59}$$

in which Ω is the excitation frequency and $J \subseteq \{1, \ldots, N_d\}$ is a set of natural frequencies considered. If we only consider the closest natural frequencies to Ω, the problem reduces to maximizing the gap between the adjacent natural frequencies. Maximizing the fundamental frequency is a special case of this problem with $\Omega = 0$.

Maximizing the gap between two natural frequencies can lead to multiple eigenfrequencies (Du and Olhoff 2007). The following example illustrates this.

Example 3: Planar Frame with Non-Structural Mass

A three-level planar frame is considered with 6 non-structural masses of 20,000kg each attached to it as shown in Figure 8a. The ratio between the stiffness of solid and void areas is reduced to $\bar{E} : \underline{E} = 100$. All other parameters are similar to example 1.

We fist maximize the fundamental frequency of the frame. The evolution history of the fundamental frequency and the final solution are shown in Figures 8b and 8c respectively. The fundamental frequency has increased by 85% from 40.2 to 74.6rad/s.

Table 1. Comparison of the results of the three approaches used to solve example 2

Approach	ω_1 (rad/s)	ω_2 (rad/s)	ω_3 (rad/s)
Using single eigenvalue sensitivities (1.18)	257.1	267.1	330.9
Using the mean eigenvalue (1.33) as objective function	248.0	424.4	540.2
Using multiple eigenvalue sensitivities (1.43)	273.5	284.0	337.6

Figure 8. Example 3: initial design (a), final solution (b), and evolution of the fundamental frequency (c)

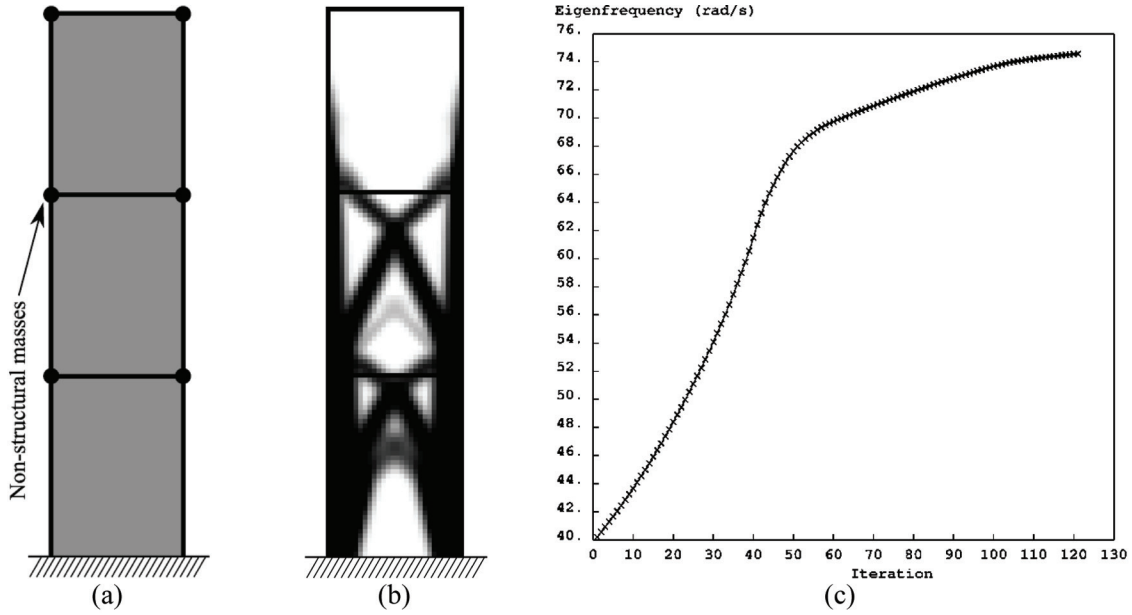

The first four natural frequencies of the initial structure are $\omega_1 = 40.2$, $\omega_2 = 163$, $\omega_3 = 215$, and $\omega_4 = 326$ (rad/s). We now assume an excitation frequency of 175 rad/s which falls between the second and the third natural frequencies, and try to move the natural frequencies of the structure away from this frequency. The problem can be simplified to maximizing the gap between the second and the third natural frequencies, i.e., maximizing the following objective function

$$f = \omega_3^2 - \omega_2^2 \tag{1.60}$$

The solution procedure explained in section 5.3 has been adopted. The optimal topology and the evolution history of the first four natural frequencies are depicted in Figure 9. The optimization algorithm, tries to increase the third natural frequency while decreasing the second natural frequency. After nearly 15 iterations, the third eigenfrequency coalesced with the fourth one but this multiple eigenfrequency has been handled well by the algorithm.

7. FORCED VIBRATION

In previous sections we have focused on free vibration and did not include external forces in our formulations. This section deals with topology optimization in forced vibration where the external dynamic forces are explicitly considered in the problem formulation. Similar to previous sections we ignore damping effects, uncertainties of the forces, geometry, and materials and consider linear elastic material behavior.

Applications of topology optimization in forced vibration have been initially studied by Ma et al. (1993) and Ma et al. (1995) using a homogenization approach. Ma et al. (1995) briefly discussed the forced vibration problem under periodic loads and defined the dynamic compliance

Figure 9. Maximizing the gap between the third and the second eigenfrequencies of the frame of example 3: final solution (a) and evolution of the first four eigenfrequencies (b). The first four eigenfrequencies of the optimal structure are $\omega_1 = 74.6$, $\omega_2 = 190$, $\omega_3 = 397$, and $\omega_4 = 408$ (rad/s).

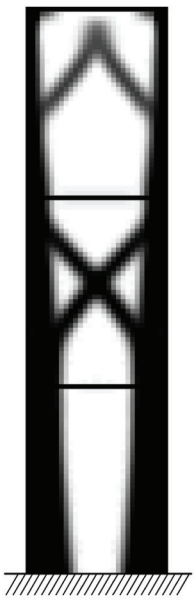

(a)

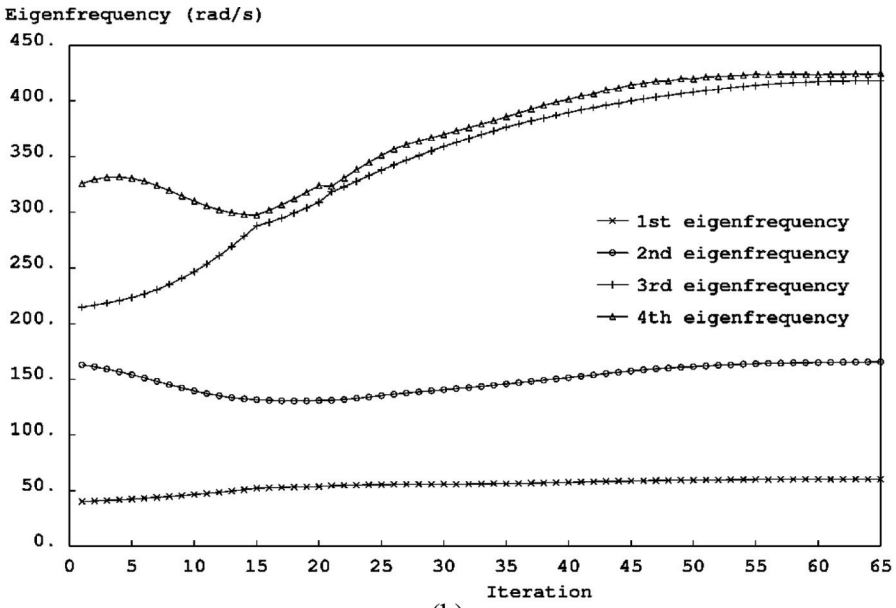

(b)

as the objective function to be minimized. Min et al. (1999) minimized the dynamic compliance for structures under impulsive loads. The topology design of structures under periodic loads has been studied more extensively by Jog (2002) where he proposed a new positive-definite definition of dynamic compliance as the average input power over a cycle. Jog (2002) also studied the problem of minimizing the vibration amplitude at certain control points. Topology design of structures subjected to design-dependent dynamic loads (e.g. hydrodynamic pressure loading) has been addressed by Olhoff and Du (2005). In more recent publications in this area, alternative approaches in using topology optimization to control the structural responses in a frequency interval has been studied by Jensen (2007) and Yoon (2010b).

Consider a harmonic external force of form

$$\mathbf{p} = \mathbf{p}_C \cos \Omega t \tag{1.61}$$

where $\mathbf{p}_C$ does not depend on time. The equation of motion for a discretized undamped system in forced vibration takes the form

$$\mathbf{M}\ddot{\mathbf{u}} + \mathbf{K}\mathbf{u} = \mathbf{p}_C \cos \Omega t \tag{1.62}$$

To solve this problem, we consider $\mathbf{u} = \mathbf{u}_C \cos\Omega t$ using which in Equation (1.62) gives

$$\left(\mathbf{K} - \Omega^2\mathbf{M}\right)\mathbf{u}_C = \mathbf{p}_C \tag{1.63}$$

or

$$\left(\mathbf{K} - \Omega^2\mathbf{M}\right)\mathbf{u} = \mathbf{p} \tag{1.64}$$

Comparing with equilibrium equation in static state, $\mathbf{K} - \Omega^2\mathbf{M}$ can be termed as "dynamic stiffness". Note that unlike the static stiffness, the dynamic stiffness matrix is not necessarily positive definite.

7.1. Objective Function and Problem Formulation

Under static loads, the compliance defined as

$$c = \mathbf{p}^T\mathbf{u} \tag{1.65}$$

is proportional to the strain energy of the structure and is a typical objective function used in topology optimization of structures. Minimizing the compliance maximizes the stiffness of the structure. Under dynamic loads, the value of c defined in Equation (1.65) varies with time. For structures subjected to periodic loads, we consider the average of c over a cycle, i.e.

$$\overline{c} = \frac{\Omega}{2\pi}\int_0^{2\pi/\Omega} \mathbf{p}^T\mathbf{u}\mathrm{d}t \tag{1.66}$$

as the objective function to be minimized. Here $T = 2\pi/\Omega$ is the time period. Note that this measure is not always positive, and thus, in problem formulation, one should consider the absolute value (or square) of average compliance as the objective function. Otherwise, for $\overline{c} < 0$, the optimization algorithm will push the structure towards resonance.

In absence of damping, $\mathbf{u} = \mathbf{u}_C \cos\Omega t$. Using this and $\mathbf{p} = \mathbf{p}_C \cos\Omega t$ in Equation (1.66), we can write

$$\overline{c} = \frac{\Omega\mathbf{p}_C^T\mathbf{u}_C}{2\pi}\int_0^{2\pi/\Omega} \cos^2 \Omega t\, dt = \frac{1}{2}\mathbf{p}_C^T\mathbf{u}_C \tag{1.67}$$

The average compliance minimization problem can now be formulated as follows

$$\begin{aligned} \min_{x_1,x_2,\ldots,x_N} \quad & c_m = 2\left|\overline{c}\right| = \left|\mathbf{p}_C^T\mathbf{u}_C\right| \\ \text{such that} \quad & \left(\mathbf{K} - \Omega^2\mathbf{M}\right)\mathbf{u}_C = \mathbf{p}_C \\ & \sum_{e=1}^{N} x_e v_e \le \overline{v} \\ & 0 < x_{\min} \le x_e \le 1, e = 1,2,\ldots,N \end{aligned} \tag{1.68}$$

7.2. Sensitivity Analysis

In order to calculate the sensitivities, we rewrite the dynamic compliance by adding an (arbitrary) adjoint vector multiplied by a zero function

$$c_m = \left|\mathbf{p}_C^T \mathbf{u}_C\right| + \tilde{\mathbf{u}}^T \left[\left(\mathbf{K} - \Omega^2 \mathbf{M}\right)\mathbf{u}_C - \mathbf{p}_C\right] \tag{1.69}$$

Differentiating with respect to the design variables and rearranging the terms, we obtain

$$\frac{\partial c_m}{\partial x_e} = \left[\text{sign}(\overline{c})\mathbf{p}_C^T + \tilde{\mathbf{u}}^T\left(\mathbf{K} - \Omega^2\mathbf{M}\right)\right]\frac{\partial \mathbf{u}_C}{\partial x} + \tilde{\mathbf{u}}^T\left(\frac{\partial \mathbf{K}}{\partial x} - \Omega^2\frac{\partial \mathbf{M}}{\partial x}\right)\mathbf{u}_C \tag{1.70}$$

where sign() is the sign function. Sensitivities of the dynamic compliance can now be written as

$$\frac{\partial c_m}{\partial x_e} = \tilde{\mathbf{u}}^T\left(\frac{\partial \mathbf{K}}{\partial x} - \Omega^2\frac{\partial \mathbf{M}}{\partial x}\right)\mathbf{u}_C \tag{1.71}$$

in which the adjoint vector is selected such that

$$\left(\mathbf{K} - \Omega^2\mathbf{M}\right)\tilde{\mathbf{u}} = -\text{sign}(\overline{c})\mathbf{p}_C \tag{1.72}$$

Comparing Equation (1.72) with Equation (1.63), the adjoint vector is found to be $\tilde{\mathbf{u}} = -\text{sign}(\mathbf{p}_C^T\mathbf{u}_C)\mathbf{u}_C$ which can be substituted in Equation (1.71) to simplify the latter to

$$\frac{\partial c_m}{\partial x_e} = -\text{sign}(\overline{c})\mathbf{u}_C^T\left(\frac{\partial \mathbf{K}}{\partial x} - \Omega^2\frac{\partial \mathbf{M}}{\partial x}\right)\mathbf{u}_C \tag{1.73}$$

Having the sensitivities calculated, an appropriate solution method such as the method of moving asymptotes (MMA) can be employed to solve the minimization problem. One can also use the OC-based solution procedure proposed in section 4.2. The optimality criteria to solve Problem (1.68) can be expressed as

$$D_e = -\frac{\partial c_m}{\partial x_e} - \Gamma v_e = \gamma_e, \quad e = 1,\ldots,N \tag{1.74}$$

with additional conditions similar to (1.21). The negative sign for $\partial c_m/\partial x$ in Equation (1.74) is added because it relates to a minimization problem.

7.3. Examples

The frame in example 3 is considered under forced vibration. It is assumed that 6 identical horizontal periodic loads of magnitude p_1 = 500 kN and frequency of Ω are applied at locations of the concentrated masses as shown in Figure 10a. Note that for linear elastic materials, changing the force magnitude will only change the values of the objective function but the evolution pattern of the objective function values and the final topology will remain unchanged. This is not true for nonlinear problems.

Deformed shapes of optimum topologies obtained for different load frequencies are shown in Figure 10b-e. It can be seen that for high frequencies, the optimum material distribution tends to form damping masses.

When the input frequency is greater than the fundamental frequency of the initial structure, the optimization algorithm reduces the fundamental frequency. This increases the static compliance and can lead to disintegrated designs (clearly observable in Figure 10e). To prevent this disintegration, one can introduce an upper bound condition on static compliance in the problem formulation (Olhoff and Du 2005). One can also include the static compliance in the objective function as shown in Figure 10.

When the structure is subjected to a number of loads with different frequencies, one can define a multi-objective optimization problem to handle the case. This is of practical importance, for example when one approximates a periodic load using Fourier series. In the following example,

Figure 10. Minimizing the dynamic compliance of the frame of example 3 under periodic loading: external periodic loads (a), and deformed shape of final topologies for different input frequencies; Ω = 0 (static loading) (b), Ω = 60 rad/s (c), Ω = 175 rad/s (d), and Ω = 330 rad/s (e). The first four natural frequencies of the initial structure are ω_1 = 40.2, ω_2 = 163, ω_3 = 215, and ω_4 = 326 (rad/s).

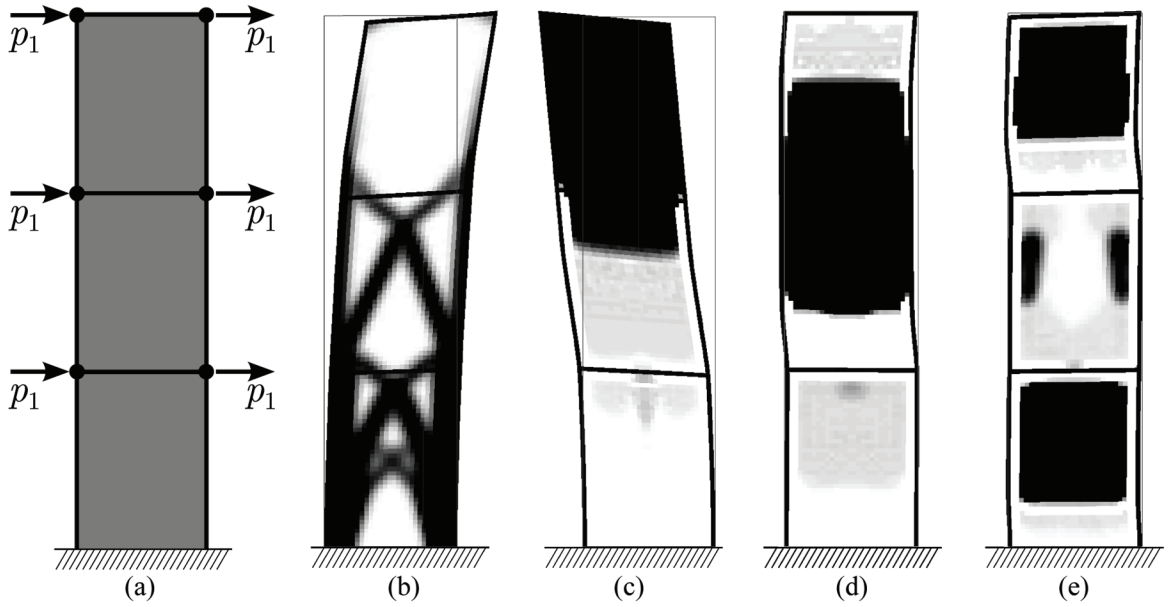

we consider the structure to be subjected to a periodic load $\mathbf{p}_1 = \mathbf{p}_{C_1} \cos \Omega t$ and a static load $\mathbf{p}_2$ (with frequency of zero). The objective function is considered as

$$c_m = \left| \mathbf{p}_{C_1}^T \mathbf{u}_{C_1} \right| + \mathbf{p}_2^T \mathbf{u}_2 \tag{1.75}$$

where

$$\left(\mathbf{K} - \Omega^2 \mathbf{M} \right) \mathbf{u}_{C_1} = \mathbf{p}_{C_1} \quad \text{and} \quad \mathbf{K}\mathbf{u}_2 = \mathbf{p}_2 \tag{1.76}$$

Sensitivities of this objective function can be calculated as

$$\frac{\partial c_m}{\partial x} = -\operatorname{sign}(\mathbf{p}_{C_1}^T \mathbf{u}_{C_1}) \mathbf{u}_{C_1}^T \left(\frac{\partial \mathbf{K}}{\partial x} - \Omega^2 \frac{\partial \mathbf{M}}{\partial x} \right) \mathbf{u}_{C_1} - \mathbf{u}_2^T \frac{\partial \mathbf{K}}{\partial x} \mathbf{u}_2 \tag{1.77}$$

The previous example is considered under the dynamic loads ($\mathbf{p}_1$) in Figure 10a and the static loads ($\mathbf{p}_2$) shown in Figure 11a. The ratio between the magnitude of the loads is p_2:p_1 = 5. Various optimal topologies resulted from using various input frequencies of $\mathbf{p}_1$ are illustrated in Figure 11b-e.

In a similar manner one can optimize the topology of a structure under any combination of static and periodic loads with different frequencies.

8. OTHER CONSIDERATIONS

So far we have simplified the optimization problems by ignoring the damping effects and nonlinear material behavior. We have also limited our study to small deformations. Considering large deformations will lead to geometrically non-linear problems.

Figure 11. Minimizing the dynamic compliance of the frame of example 3 under a combination of periodic loading of Figure 10a and static loading: external static loads (a), and final topologies for different input frequencies of the periodic load; Ω = 0 (b), Ω = 60 rad/s (c), Ω = 175 rad/s (d), and Ω = 330 rad/s (e)

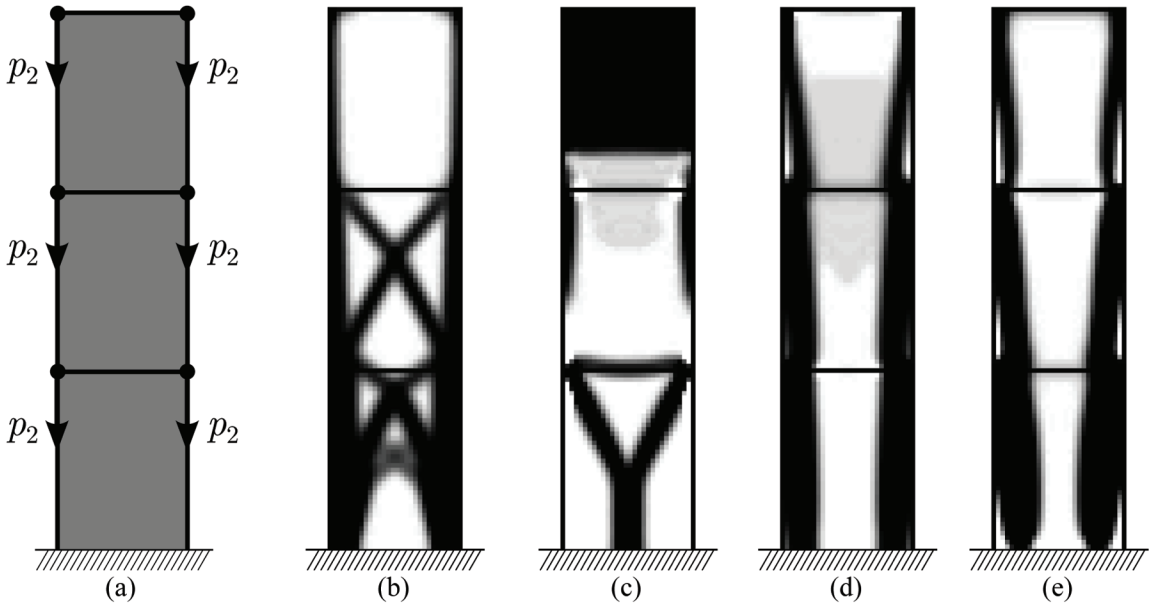

Including either geometrical or material non-linearity in problems causes the stiffness matrix to be load-dependent. The equilibrium equations in such problems are commonly solved by the Newton-Raphson method. Finding eigenfrequencies will require a subsequent modal analysis.

Sensitivity analysis of a general displacement-based functional in a geometrically and materially non-linear system has been formulated by Jung and Gea (2004). This formulation can be used to calculate sensitivities of compliance-like objective functions. Similar procedure of deriving the sensitivities of an energy functional for a non-linear system is presented in Section 9.1.

In geometrically non-linear problems, the extremely soft "void" elements of the SIMP material model can be troublesome showing zero or even negative tangent stiffness and causing serious convergence problems (see e.g. Buhl et al. 2000). A new approach called Element Connectivity Parameterization has been proposed by Yoon and Kim (2005) to address this problem. This approach proves to be useful in topology optimization of non-linear structures under dynamic loads (Yoon 2010a, 2011). Another approach to solve this issue is eliminating the void elements (see Section 9.1).

Considering damping effects will also change the sensitivities of the objective functions considered. In the following we update the previously derived sensitivities in presence of damping.

8.1. Forced Vibration with Damping

The equation of motion under a periodic load takes the form

$$\mathbf{M}\ddot{\mathbf{u}} + \mathbf{C}\dot{\mathbf{u}} + \mathbf{K}\mathbf{u} = \mathbf{p} = \mathbf{p}_C \cos\Omega t \qquad (1.78)$$

Introducing the complex displacement $\mathbf{z} = \left(\mathbf{z}_C + i\mathbf{z}_S\right)e^{i\Omega t}$, and assuming $\mathbf{u}$ to be the real part of $\mathbf{z}$, we rewrite this equation in the complex space as

$$\mathbf{M}\ddot{\mathbf{z}} + \mathbf{C}\dot{\mathbf{z}} + \mathbf{K}\mathbf{z} = \mathbf{p}_C e^{i\Omega t} \tag{1.79}$$

Separating the real and imaginary parts, we obtain

$$\begin{cases} \mathbf{B}\mathbf{z}_C - \Omega\mathbf{C}\mathbf{z}_S = \mathbf{p}_c \\ \mathbf{B}\mathbf{z}_S + \Omega\mathbf{C}\mathbf{z}_C = 0 \end{cases} \tag{1.80}$$

where $\mathbf{B} = \mathbf{K} - \Omega^2\mathbf{M}$. Calculating $\mathbf{z}_S$ from the second equation in (1.80) yields

$$\mathbf{z}_S = -\Omega\mathbf{B}^{-1}\mathbf{C}\mathbf{z}_C \tag{1.81}$$

After substituting in the first equation in (1.80), we get

$$\hat{\mathbf{K}}\mathbf{z}_C = \mathbf{p}_C \tag{1.82}$$

where

$$\hat{\mathbf{K}} = \mathbf{B} + \Omega^2\mathbf{C}\mathbf{B}^{-1}\mathbf{C} \tag{1.83}$$

The displacement vector $\mathbf{u}$ is the real part of $\mathbf{z}$, so

$$\mathbf{u} = \Re\left(\left(\mathbf{z}_C + i\mathbf{z}_S\right)e^{i\Omega t}\right) = \left(\cos\Omega t\right)\mathbf{z}_C - \left(\sin\Omega t\right)\mathbf{z}_S \tag{1.84}$$

Using this and $\mathbf{p} = \mathbf{p}_C \cos\Omega t$ in Equation (1.66), we can write

$$\bar{c} = \frac{\Omega}{2\pi}\int_0^{2\pi/\Omega}\left(\mathbf{p}_C^T\mathbf{z}_C\cos^2\Omega t - \mathbf{p}_C^T\mathbf{z}_s\cos\Omega t\sin\Omega t\right)dt = \frac{1}{2}\mathbf{p}_C^T\mathbf{z}_C \tag{1.85}$$

Differentiating with respect to design variable x_e, we obtain

$$\frac{\partial\bar{c}}{\partial x_e} = \frac{1}{2}\mathbf{p}_C^T\frac{\partial\mathbf{z}_C}{\partial x_e} \tag{1.86}$$

But from Equation (1.82),

$$\frac{\partial\hat{\mathbf{K}}}{\partial x_e}\mathbf{z}_C + \hat{\mathbf{K}}\frac{\partial\mathbf{z}_C}{\partial x_e} = 0 \quad \Rightarrow \quad \hat{\mathbf{K}}\frac{\partial\mathbf{z}_C}{\partial x_e} = -\frac{\partial\hat{\mathbf{K}}}{\partial x_e}\mathbf{z}_C \tag{1.87}$$

which can be used in Equation (1.86) to yield

$$\frac{\partial\bar{c}}{\partial x_e} = \frac{1}{2}\mathbf{p}_C^T\frac{\partial\mathbf{z}_C}{\partial x_e} = \frac{1}{2}\mathbf{z}_C^T\hat{\mathbf{K}}\frac{\partial\mathbf{z}_C}{\partial x_e} = -\frac{1}{2}\mathbf{z}_C^T\frac{\partial\hat{\mathbf{K}}}{\partial x_e}\mathbf{z}_C \tag{1.88}$$

We thus need to calculate $\partial\hat{\mathbf{K}} / \partial x_e$. Before proceeding we note that

$$\mathbf{B}^{-1}\mathbf{B} = \mathbf{I} \quad \Rightarrow \quad \frac{\partial\mathbf{B}^{-1}}{\partial x_e}\mathbf{B} + \mathbf{B}^{-1}\frac{\partial\mathbf{B}}{\partial x_e} = 0 \quad \Rightarrow \quad \frac{\partial\mathbf{B}^{-1}}{\partial x_e} = -\mathbf{B}^{-1}\frac{\partial\mathbf{B}}{\partial x_e}\mathbf{B}^{-1} \tag{1.89}$$

in which we used the fact that $\mathbf{B}$ is symmetric, i.e. $\mathbf{B}^T = \mathbf{B}$. Differentiating Equation (1.83) and making use of Equation (1.89) and symmetry of $\mathbf{B}$ and $\mathbf{C}$, we obtain

$$\frac{\partial\hat{\mathbf{K}}}{\partial x_e} = \frac{\partial\mathbf{B}}{\partial x_e} - \Omega^2\mathbf{C}\mathbf{B}^{-1}\frac{\partial\mathbf{B}}{\partial x_e}\mathbf{B}^{-1}\mathbf{C} + 2\Omega^2\frac{\partial\mathbf{C}}{\partial x_e}\mathbf{B}^{-1}\mathbf{C} \tag{1.90}$$

Pre- and post-multiplying by $\mathbf{z}_C$ and using Equation (1.81), we achieve

$$\mathbf{z}_C^T\frac{\partial\hat{\mathbf{K}}}{\partial x_e}\mathbf{z}_C = \mathbf{z}_C^T\frac{\partial\mathbf{B}}{\partial x_e}\mathbf{z}_C - \mathbf{z}_S^T\frac{\partial\mathbf{B}}{\partial x_e}\mathbf{z}_S - 2\Omega\mathbf{z}_C^T\frac{\partial\mathbf{C}}{\partial x_e}\mathbf{z}_S \tag{1.91}$$

Substituting in Equation (1.88) and replacing $\mathbf{B}$ by $\mathbf{K} - \Omega^2\mathbf{M}$, we obtain

$$\frac{\partial\bar{c}}{\partial x_e} = \frac{1}{2}\left[\mathbf{z}_S^T\left(\frac{\partial\mathbf{K}}{\partial x_e} - \Omega^2\frac{\partial\mathbf{M}}{\partial x_e}\right)\mathbf{z}_S - \mathbf{z}_C^T\left(\frac{\partial\mathbf{K}}{\partial x_e} - \Omega^2\frac{\partial\mathbf{M}}{\partial x_e}\right)\mathbf{z}_C\right] + \Omega\mathbf{z}_C^T\frac{\partial\mathbf{C}}{\partial x_e}\mathbf{z}_S \tag{1.92}$$

If we now define the objective function as $c_m = 2\left|\overline{c}\right|$, for the sensitivities of this function we can write

$$\frac{\partial c_m}{\partial x_e} = \text{sign}(\overline{c}) \begin{bmatrix} \mathbf{z}_S^T \left(\frac{\partial \mathbf{K}}{\partial x_e} - \Omega^2 \frac{\partial \mathbf{M}}{\partial x_e} \right) \mathbf{z}_S - \\ \mathbf{z}_C^T \left(\frac{\partial \mathbf{K}}{\partial x_e} - \Omega^2 \frac{\partial \mathbf{M}}{\partial x_e} \right) \mathbf{z}_C + 2\Omega \mathbf{z}_C^T \frac{\partial \mathbf{C}}{\partial x_e} \mathbf{z}_S \end{bmatrix} \tag{1.93}$$

Ignoring damping effects, we have $\mathbf{C} = 0$, $\mathbf{z}_S = 0$, and $\mathbf{z}_C = \mathbf{u}_C$, and thus the above equation reduces to Equation (1.73).

The vectors $\mathbf{z}_C$ and $\mathbf{z}_S$ in Equation (1.93) can be obtained by solving Equation (1.80). Given the damping matrix $\mathbf{C}$, the term $\partial \mathbf{C}/\partial x_e$ is also calculable. For example, assuming the Reyliegh damping formulation of Equation (1.2), we have $\partial \mathbf{C} / \partial x_e = a_M \partial \mathbf{M} / \partial x_e + a_K \partial \mathbf{K} / \partial x_e$.Having the sensitivities, one can solve the optimization problem using a suitable solution algorithm.

8.2. Free Vibration with Damping

Using a similar approach followed in the previous section, in case of free vibration, Eqs. (1.79) and (1.80) need to be changed to

$$\mathbf{M}\ddot{\mathbf{z}} + \mathbf{C}\dot{\mathbf{z}} + \mathbf{K}\mathbf{z} = 0, \quad \mathbf{z} = \left(\mathbf{z}_C + i\mathbf{z}_S\right) e^{i\omega t}, \tag{1.94}$$

$$\begin{cases} \mathbf{B}\mathbf{z}_C - \omega \mathbf{C}\mathbf{z}_S = 0 \\ \mathbf{B}\mathbf{z}_S + \omega \mathbf{C}\mathbf{z}_C = 0 \end{cases} \tag{1.95}$$

respectively where ω is a natural frequency and

$$\mathbf{B} = \mathbf{K} - \omega^2 \mathbf{M} \tag{1.96}$$

From the second equation in (1.95), for $\mathbf{z}_S$ we can write

$$\mathbf{z}_S = -\omega \mathbf{B}^{-1} \mathbf{C} \mathbf{z}_C \tag{1.97}$$

which after substituting in the first equation of (1.95), gives

$$\hat{\mathbf{K}}\mathbf{z}_C = 0, \quad \hat{\mathbf{K}} = \mathbf{B} + \omega^2 \mathbf{C}\mathbf{B}^{-1}\mathbf{C} \tag{1.98}$$

Using Equation (1.98), we can now write

$$\frac{\partial \hat{\mathbf{K}}}{\partial x_e} \mathbf{z}_C = -\hat{\mathbf{K}} \frac{\partial \mathbf{z}_C}{\partial x_e} \quad \Rightarrow \quad \mathbf{z}_C^T \frac{\partial \hat{\mathbf{K}}}{\partial x_e} \mathbf{z}_C = -\mathbf{z}_C^T \hat{\mathbf{K}} \frac{\partial \mathbf{z}_C}{\partial x_e} = 0 \tag{1.99}$$

Differentiating Equation (1.98), we get

$$\frac{\partial \hat{\mathbf{K}}}{\partial x_e} = \frac{\partial \mathbf{B}}{\partial x_e} + 2\omega^2 \frac{\partial \mathbf{C}}{\partial x_e} \mathbf{B}^{-1}\mathbf{C} - \omega^2 \mathbf{C}\mathbf{B}^{-1} \frac{\partial \mathbf{B}}{\partial x_e} \mathbf{B}^{-1}\mathbf{C} + 2\omega \frac{\partial \omega}{\partial x_e} \mathbf{C}\mathbf{B}^{-1}\mathbf{C} \tag{1.100}$$

Pre- and post-multiplying this equation by $\mathbf{z}_C$ and using Equation (1.97), we obtain

$$\mathbf{z}_C^T \frac{\partial \hat{\mathbf{K}}}{\partial x_e} \mathbf{z}_C = \mathbf{z}_C^T \frac{\partial \mathbf{B}}{\partial x_e} \mathbf{z}_C - 2\omega \mathbf{z}_C \frac{\partial \mathbf{C}}{\partial x_e} \mathbf{z}_S - \mathbf{z}_S^T \frac{\partial \mathbf{B}}{\partial x_e} \mathbf{z}_S - 2 \frac{\partial \omega}{\partial x_e} \mathbf{z}_C^T \mathbf{C}\mathbf{z}_S = 0 \tag{1.101}$$

Differentiating Equation (1.96), we have

$$\frac{\partial \mathbf{B}}{\partial x_e} = \frac{\partial \mathbf{K}}{\partial x_e} - \omega^2 \frac{\partial \mathbf{M}}{\partial x_e} - 2\omega \frac{\partial \omega}{\partial x_e} \mathbf{M} \tag{1.102}$$

Substituting this equation in Equation (1.101) and rearranging yields

$$\frac{\partial \omega}{\partial x_e} = \frac{\mathbf{z}_C^T \left(\frac{\partial \mathbf{K}}{\partial x_e} - \omega^2 \frac{\partial \mathbf{M}}{\partial x_e} \right) \mathbf{z}_C - \mathbf{z}_S^T \left(\frac{\partial \mathbf{K}}{\partial x_e} - \omega^2 \frac{\partial \mathbf{M}}{\partial x_e} \right) \mathbf{z}_S - 2\omega \mathbf{z}_C \frac{\partial \mathbf{C}}{\partial x_e} \mathbf{z}_S}{2\left(\mathbf{z}_C^T \mathbf{C} \mathbf{z}_S + \omega \mathbf{z}_C^T \mathbf{M} \mathbf{z}_C + \omega \mathbf{z}_S^T \mathbf{M} \mathbf{z}_S \right)} \tag{1.103}$$

If we normalize the vectors $\mathbf{z}_C$ and $\mathbf{z}_S$ with respect to $\mathbf{M}$, for sensitivities of $\lambda = \omega^2$, we can write

$$\frac{\partial \lambda}{\partial x_e} = 2\omega \frac{\partial \omega}{\partial x_e} = \frac{\mathbf{z}_C^T \left(\frac{\partial \mathbf{K}}{\partial x_e} - \omega^2 \frac{\partial \mathbf{M}}{\partial x_e} \right) \mathbf{z}_C - \mathbf{z}_S^T \left(\frac{\partial \mathbf{K}}{\partial x_e} - \omega^2 \frac{\partial \mathbf{M}}{\partial x_e} \right) \mathbf{z}_S - 2\omega \mathbf{z}_C \frac{\partial \mathbf{C}}{\partial x_e} \mathbf{z}_S}{\frac{\mathbf{z}_C^T \mathbf{C} \mathbf{z}_S}{\omega} + 2} \tag{1.104}$$

It is easy to verify that in the without damping this equation reduces to Equation(1.18). Having the sensitivities, one can solve the optimization problem using a suitable solution algorithm.

9. MAXIMIZING ENERGY ABSORPTION

Apart from controlling natural frequencies and dynamic compliance, improving energy absorption characteristics is also of significant importance in seismic design of structures. In recent years, active and passive energy dissipating devices have been widely studied and utilized to increase energy absorption of structural systems (Soong and Spencer 2002). Topology optimization can be used to maximize energy absorption of these devices. In this section we consider the problem of maximizing the energy absorption of passive energy dissipaters which make use of yield deformation of metals to mitigate the excitation energy. These kinds of energy dissipating devices are popular due to low cost of fabrication and maintenance and easy installation (Ghabraie et al. 2010).

We consider an energy damping device which is made of a 100 mm-long cut of a standard structural wide-flange section with depth, flange width, web thickness, and flange thickness of 161.8, 152.2, 8, and 11.5 mm respectively. This device can be installed in braces connections (Chan and Albermani 2008) or beam-column connections (Oh et al. 2009) as depicted in Figure 12a. In these installations the device will deform mainly in shear (Figure 12a). The design domain is the inner part of the web as shown in Figure 12b. The two 15 mm strips on the boundaries of the web are non-designable.

We use the BESO method here and introduce a simple technique to solve shape optimization problems using BESO. Restricting the topology of the design and performing shape optimization instead of topology optimization is useful when the fabrication cost is an important factor. We also address a simple approach to obtain periodic designs which are produced by repeating a fixed pattern.

Considering a volume constraint, the energy absorption maximization problem can be stated as

$$\begin{aligned} \max_{x_1, x_2, \ldots, x_N} \quad & \Pi_p \\ \text{such that} \quad & \mathbf{r} = \mathbf{p} - \hat{\mathbf{p}} = 0 \\ & \sum_{e=1}^{N} x_e v_e = \overline{v} \\ & 0 \le x_e \le 1, \qquad e = 1, 2, \ldots, N \end{aligned} \tag{1.105}$$

where Π_p is the total plastic dissipation. Because the problem involves plastic behavior, one needs to solve a non-linear equilibrium system of the form

$$\mathbf{r} = \mathbf{p} - \hat{\mathbf{p}} = 0 \tag{1.106}$$

This requires an iterative solver to eliminate the residual force vector $\mathbf{r}$ defined as the difference between the external and internal force vectors, $\mathbf{p}$ and $\hat{\mathbf{p}}$ respectively.

The internal force vector is defined as

$$\hat{\mathbf{p}} = \sum_{e=1}^{N} \int_{v_e} \mathbf{G}_e^T \mathbf{B}_e^T \sigma_e \, \mathrm{d}v = \sum_{e=1}^{N} \mathbf{G}_e^T \mathbf{q}_e \tag{1.107}$$

Figure 12. A passive energy dissipating device: (a) Installation and deformation; (b) designable and non-designable domains and loading. Dimensions are in mm

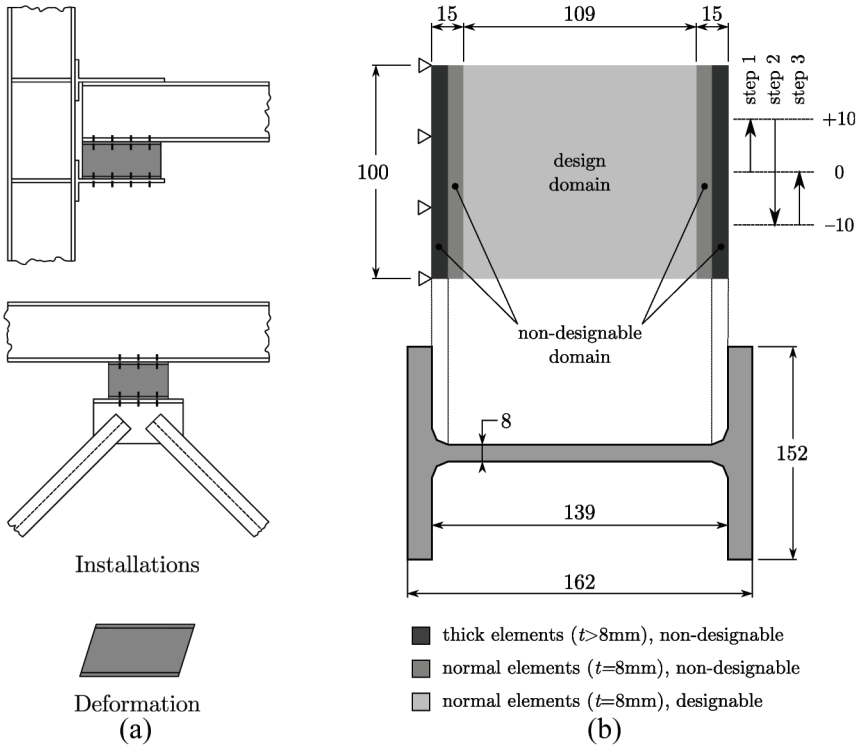

where $\mathbf{G}_e$ is the matrix that transforms the local nodal values of element e to the global nodal values, $\mathbf{B}$ is the strain-displacement matrix and $\boldsymbol{\sigma}$ represents the local element stress vector. The stress vector can be expressed as

$$\boldsymbol{\sigma}_e = \mathbf{D}_e \boldsymbol{\varepsilon}_e \tag{1.108}$$

with $\boldsymbol{\varepsilon}$ being the strain vector and $\mathbf{D}$ the stress-strain matrix. Similar to Eqs. (1.10) and (1.12) we can define the relationship between $\mathbf{D}$ and the design variables in the following form

$$\mathbf{D}_e(x_e) = x_e \bar{\mathbf{D}}_e \tag{1.109}$$

in which $\bar{\mathbf{D}}_e$ is the stress-strain matrix of element e in its solid state.

We consider the energy damping device to undergo a full loading cycle consisting of an upward displacement of 10 mm followed by a 20 mm downward displacement and finally a 10 mm upward displacement to its original position (Figure 12b). Due to this loading, the total plastic dissipation would be equal to the total strain energy

$$\Pi_p = \Pi = \oint \mathbf{p} \cdot \mathrm{d}\,\mathbf{u} = \sum_{e=1}^{N} \oint \mathbf{p}_e \cdot \mathrm{d}\,\mathbf{u}_e \tag{1.110}$$

Using the trapezoidal rule for integration, (1.110) can be written in the form

$$\Pi_p = \lim_{n\to\infty} \frac{1}{2} \sum_{i=1}^{n} \left(\mathbf{u}_{(i)}^T - \mathbf{u}_{(i-1)}^T\right)\left(\mathbf{p}_{(i)} + \mathbf{p}_{(i-1)}\right) \tag{1.111}$$

where the subscripts in parentheses indicate the integration divisions.

9.1. Bidirectional Evolutionary Structural Optimization (BESO)

The BESO method has been used in eigenfrequency optimization (see e.g. Yang et al. 1999b, Huang et al. 2010) as well as in maximizing energy absorption (see e.g. Huang et al. 2007, Ghabraie et al. 2010). This method solves the topology optimization problem in two steps. At first, the optimization algorithm finds the most and least efficient elements to be added and removed respectively. Then, it adjusts the number of adding and removing elements based on the volume constraint.

This method is capable of totally removing the elements, hence one does not require to represent voids with a very soft material. This approach, usually known as *hard kill* approach, results in faster solutions for only solid elements remain in the finite element model. Moreover, this approach works well in geometrically non-linear problems as it is not prone to the instabilities caused by soft elements in the SIMP material model (Buhl et al. 2000, Yoon and Kim 2005). Zhou and Rozvany (2001) showed that in certain cases the hard kill approach may result in non-optimal solutions and thus this approach need to be applied with care. In shape optimization, however, using the hard kill approach will not cause such problems.

Another advantage of the BESO method is that the solutions will not contain any intermediate design variables ($0 < x < 1$) or grey areas. In this method the boxing constraints $0 \le x_e \le 1$, $e = 1,\ldots,N$ change to binary constraints of the form $x_e \in \{0,1\}$, $e = 1,\ldots,N$. This is particularly helpful if one wants to impose shape restrictions as the boundaries of solids and voids can be clearly defined in the black-white solutions of BESO.

In BESO, the so-called *sensitivity numbers* are used to evaluate the efficiency of the elements. Sensitivity numbers might be assigned intuitively or calculated rigorously. Either way, they are defined such that a higher sensitivity number represents higher efficiency.

Considering the definition of the objective function in Equation (1.111), the sensitivities of this function can be calculated as

$$\frac{\partial \Pi_p}{\partial x_e} = \lim_{n\to\infty} \frac{1}{2} \sum_{i=1}^{n} \left[\left(\frac{\partial \mathbf{u}_{(i)}^T}{\partial x_e} - \frac{\partial \mathbf{u}_{(i-1)}^T}{\partial x_e} \right) \left(\mathbf{p}_{(i)} + \mathbf{p}_{(i-1)} \right) + \left(\mathbf{u}_{(i)}^T - \mathbf{u}_{(i-1)}^T \right) \left(\frac{\partial \mathbf{p}_{(i)}}{\partial x_e} + \frac{\partial \mathbf{p}_{(i-1)}}{\partial x_e} \right) \right] \tag{1.112}$$

The first term in the right hand side cancels out because on the boundaries with essential boundary conditions $\partial \mathbf{u}/\partial x = 0$ and elsewhere $\mathbf{p} = 0$. Hence the above equation reduces to

$$\frac{\partial \Pi_p}{\partial x_e} = \lim_{n\to\infty} \frac{1}{2} \sum_{i=1}^{n} \left(\mathbf{u}_{(i)}^T - \mathbf{u}_{(i-1)}^T \right) \left(\frac{\partial \mathbf{p}_{(i)}}{\partial x_e} + \frac{\partial \mathbf{p}_{(i-1)}}{\partial x_e} \right) \tag{1.113}$$

On the other hand, differentiating Equation (1.106) and using Eqs. (1.107) to (1.109), we obtain

$$\frac{\partial \mathbf{p}}{\partial x_e} = \frac{\partial \hat{\mathbf{p}}}{\partial x_e} = \mathbf{G}_e^T \mathbf{q}_e, \quad e = 1,\ldots,N \tag{1.114}$$

Substituting Equation (1.114) in Equation (1.113), we can write

$$\frac{\partial \Pi_p}{\partial x_e} = \lim_{n\to\infty} \frac{1}{2} \sum_{i=1}^{n} \left(\mathbf{u}_{(i)}^T - \mathbf{u}_{(i-1)}^T \right) \mathbf{G}_e^T \left(\mathbf{q}_{e(i)} + \mathbf{q}_{e(i-1)} \right) \tag{1.115}$$

Using the trapezoidal numerical integration scheme and recalling the definition of the strain energy in Eqs. (1.110) and (1.111), the above equation reduces to

$$\frac{\partial \Pi_p}{\partial x_e} = \lim_{n\to\infty} \sum_{i=1}^{n} \left(\pi_{e(i)} - \pi_{e(i-1)} \right) = \pi_e \tag{1.116}$$

where π_e is the total strain energy of element e upon completion of the load cycle. Huang and Xie (2008) derived these sensitivities using the adjoint method and verified it using a simple example.

We may now define the sensitivity numbers for problem (1.105) as follows

$$\alpha_e = \frac{\partial \Pi_p}{\partial x_e} = \pi_e, \qquad e = 1, 2, \ldots, N \quad (1.117)$$

Based on this definition and using first order approximation, we can write

$$\Delta \Pi_p = \sum_{e=1}^{N} \alpha_e \Delta x_e \quad (1.118)$$

Note that in Equation (1.118) adding element e will be reflected by $\Delta x_e = 1 - 0 = 1$ and removing it results in $\Delta x_e = -1$. Thus during the solution procedure, if one introduces the ath element and removes the rth element, the change in the objective function can be estimated as

$$\Delta \Pi_p = \frac{\partial \Pi_p}{\partial x_a} - \frac{\partial \Pi_p}{\partial x_r} = \alpha_a - \alpha_r \quad (1.119)$$

As we are interested in maximizing Π_p it is clear from Equation (1.119) that the elements with highest sensitivity numbers should be added to the design domain while the elements with lowest sensitivity numbers should be removed.

9.2. Adding and Removing the Elements

After ranking the efficiency of the elements, the algorithm should select the number of elements to be added and removed such that the volume constraint is satisfied. Generally in BESO, one starts the solution with an initial volume which is not necessarily equal to the volume limit $\overline{v}$. The design is then updated using the sensitivity numbers and the algorithm tries to move the volume towards the volume limit gradually. Thus, if the current volume is bigger than $\overline{v}$ the algorithm will increase the number of removing elements and vice versa. The procedure continues until no further significant improvement can be achieved.

The algorithms to update the solutions in the BESO method have been improved over time. One of the most recent algorithms is proposed by Huang and Xie (2007). In this algorithm, at each iteration k, the target volume of the next iteration is calculated using a small positive controlling parameter called the *evolutionary volume ratio* (R_v)

$$v^{(k+1)} = v^{(k)} \left(1 + \text{sign}(\overline{v} - v^{(k)}) R_v\right) \quad (1.120)$$

where superscripts enclosed in parentheses indicate the iteration number. Then the number of adding and removing elements are calculated such that the volume of the next design becomes equal to $v^{(k+1)}$ and the total number of added elements do not exceed $v^{add} = v_t \times R_a$ in which R_a is another controlling parameter known as the *maximum allowable admission ratio*.

If one starts BESO with an initial design volume equal to $\overline{v}$, the volume will be kept constant during the optimization procedure and the number of adding and removing elements at each iteration would be equal to each other. In this case R_v will have no effect on the optimization procedure and the maximum number of adding and removing elements is only controlled by R_a. Thus with a fixed volume, the effect of the R_a factor is similar to the move limit η in Equation (1.28).

9.3. Mirroring and Filtering Sensitivity Numbers

Due to the nonlinear nature of Problem (1.105), the loading sequence affects the mechanical responses. As a result, the optimal shape flips by mirroring the loading sequence. In real life, how-

ever, the direction of the load is uncertain. Thus one needs to consider two displacement cycles: a ↑↓↑ cycle as well as a ↓↑↓ cycle. But knowing that the results of these two displacement cycles are mirrored images of each other, it is not necessary to analyze the model under both of these loading conditions. Instead, one can add the sensitivities of the mirrored elements together to account for both displacement cycles. The sensitivity numbers are thus corrected as

$$\bar{\alpha}_e = \alpha_e + \alpha_{\vec{e}} \tag{1.121}$$

where $\bar{\alpha}_e$ is the corrected sensitivity number of element e and $\vec{e}$ is the element which is located at the same location as e in the mirrored model.

Like the SIMP method, the BESO method is also prone to the formation of checkerboard patterns and mesh dependency. A filtering technique, similar to Equation (1.29) can be employed to overcome these problems in the BESO algorithm

$$\widehat{\alpha_e} = \frac{\sum_{e=1}^{N} \bar{\alpha}_j w_{ij}}{\sum_{j=1}^{N} w_{ij}} \tag{1.122}$$

Another significance of filtering in the BESO method is extrapolating the sensitivity numbers to void elements. If one uses a hard kill approach, void elements are removed from the structure and their sensitivities cannot be evaluated directly. In other words, all void elements will have a sensitivity number of zero. The filtering scheme in Equation (1.122) extrapolates the sensitivities to the void elements in the neighborhood of the solid elements. This extrapolation leads the BESO algorithm to add the elements in the vicinity of the elements with high sensitivity numbers.

9.4. Restricting the Topology

Topology optimization techniques like BESO can naturally introduce new holes or fill the current holes in the design domain. However this behavior might produce complicated shapes which might be costly to fabricate. To prevent the BESO algorithm from introducing new holes, we restrict the designable domain to the elements at the boundaries of the shape at each iteration. The designable domain at each iteration is defined as

$$\mathcal{D} = \left\{ e \middle| \exists i, j \in \mathcal{B} : i, j \in e \wedge i \neq j \right\} \tag{1.123}$$

where $\mathcal{B}$ is the set of boundary nodes defined as

$$\mathcal{B} = \left\{ i \middle| \exists e_m \in \mathcal{S}, e_v \in \mathcal{V} : i \in e_m \bigcap e_v \right\} \tag{1.124}$$

with $\mathcal{S}$ and $\mathcal{V}$ denoting the sets of solid and void elements respectively.

9.5. Numerical Examples

In the following numerical examples we fix the volume to simplify the approach. Another benefit of using fixed volume is that the results of different iterations are comparable to each other.

The modulus of elasticity of the material is considered as 206.1 GPa and the tensile yield stress is assumed to be 334 MPa. The material model considered is depicted in Figure 13.

Example 4: Simple Damper

We use the proposed BESO algorithm to optimize the shape of a simple damper. The target volume is 82% of the design domain. The initial and the final solutions are depicted in Figures 14a and 14b respectively. The evolution history of the objective function is plotted in Figure 14c. It can be verified that the energy absorption of the optimal solution

Figure 13. The idealized material model used for modeling the energy dissipating device

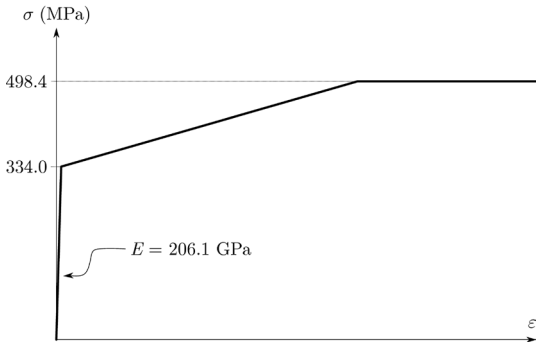

is considerably higher (37.4% improvement) than the initial design.

Example 5. Slit Damper

We now consider shape optimization of a slit damper. The initial design is depicted in Figure 14d. In order to preserve the periodicity of the design, one needs to impose an additional constraint to the optimization algorithm. To this end, we partition the design domain into four cells. To make the cells identical, the sensitivity numbers of elements are replaced by the mean value of sensitivity numbers of corresponding elements in all cells. Putting this mathematically, we write

$$\alpha_i = \frac{1}{N_{cell}} \sum_{j=1}^{N_{cell}} \alpha_{i,j} \qquad (1.125)$$

where α_i is the average (corrected) sensitivity number of element i in all cells, N_{cell} is the number of cells, and $\alpha_{i,j}$ is the (original) sensitivity number of the element i in cell j.

The obtained solution is illustrated in Figure 14e. The evolution history of the objective function is plotted in Figure 14f. Again a significant improvement (64.3%) in energy absorption is observable.

Ghabraie et al. (2010) have used a smoothing postprocessor based on Bézier curves to smooth the jagged boundaries of the solutions. The smoothed versions of the initial and optimal solution are analyzed and their stress distributions are compared in Figure 15. It can be seen that the optimal solution provides an even stress distribution and the stress concentration areas visible in the initial design have been dissipated. This even stress distribution improves the responses of this design against low cycle fatigue. This has been verified through experimental tests by Ghabraie et al. (2010).

Figure 16 compares the force-displacement curves of the initial and final solutions. The optimal solution shows a stiffer response than the initial design.

10. CONCLUSION

This chapter reviewed the application of topology optimization techniques in seismic design of structures. Two established topology optimization methods, namely SIMP and BESO, have been introduced and their application has been illustrated using numerical examples.

Eigenfrequency optimization of linear elastic structures in free vibration has been addressed using the SIMP method. Sensitivity analysis of eigenfrequencies has been explained and a simple solution procedure has been presented based on optimality criteria. Possible numerical instabilities have been mentioned and possible treatments have been discussed.

The problems involving multiple eigenfrequencies have been considered and simple approaches to bypass these problems have been discussed. The sensitivities of multiple eigenfrequencies have been calculated and the optimality criteria have been presented. A simple approach to solve these problems has been proposed and successfully applied to a simple problem. The problem of maximizing the gap between two eigenfrequencies has also been addressed. This problem is of practical significance when it is desired to push

Figure 14. Solutions of examples 4 and 5. The initial designs (a,d), the final designs (b,e), and the evolution history of the objective functions (c,f). Dark grey elements are non-designable

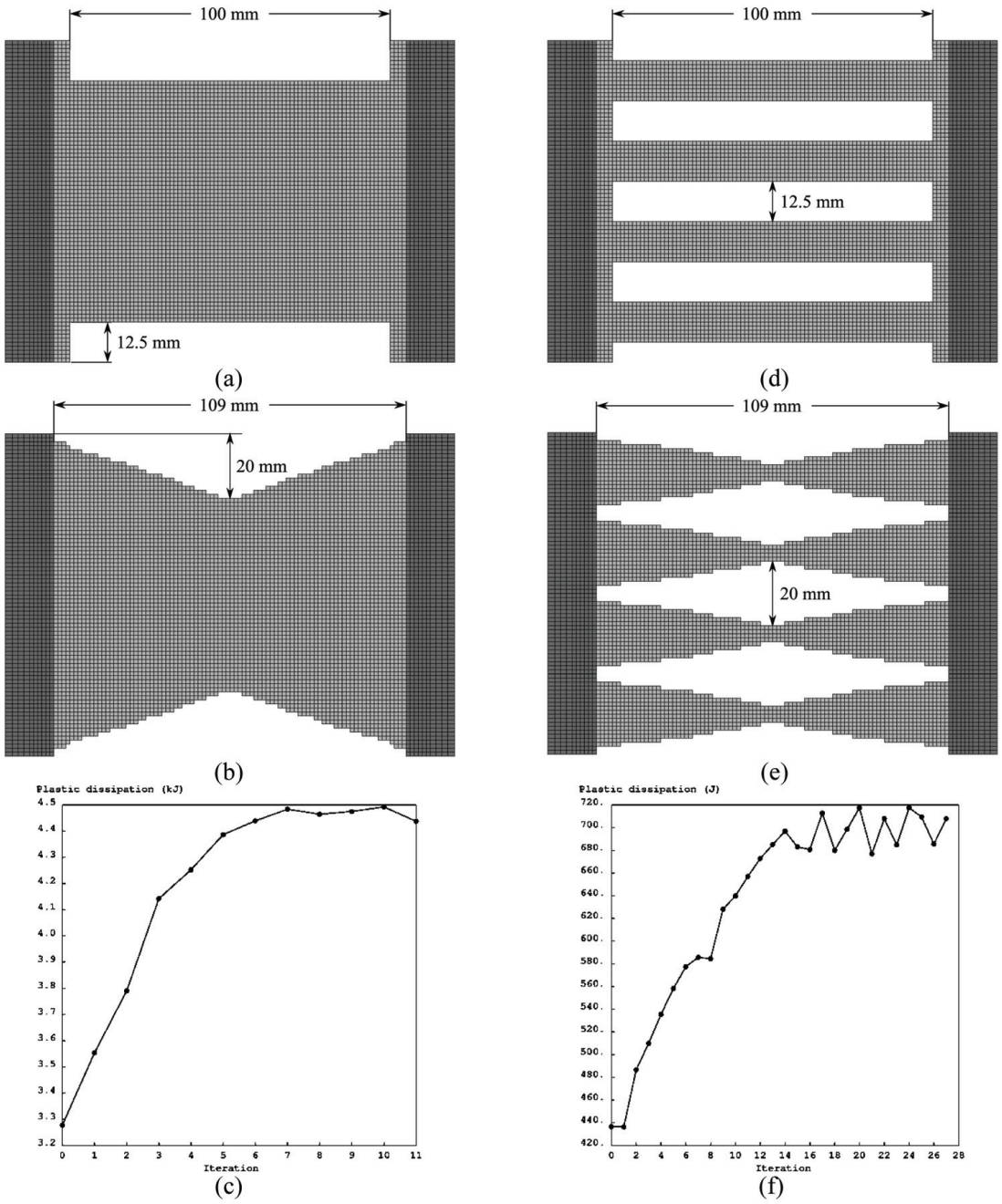

Figure 15. Comparing stress distribution in initial (a) and final (b) smoothed designs. Stresses are in MPa.

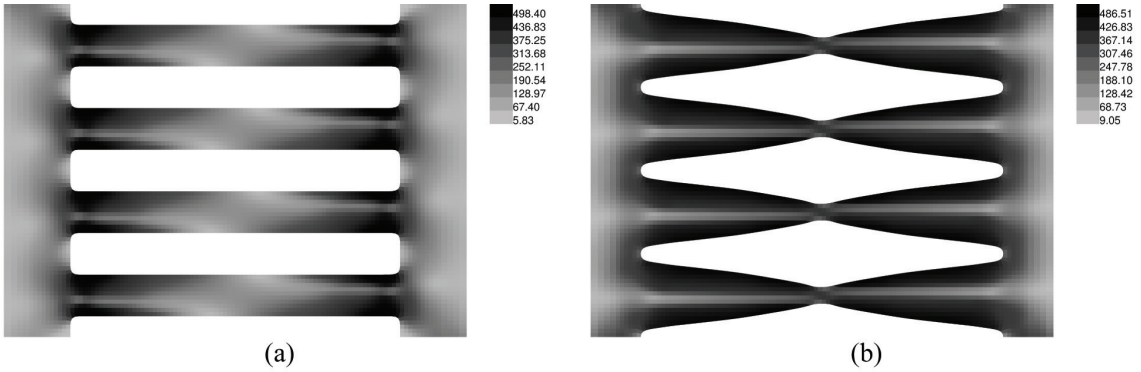

Figure 16. Comparing force-displacement graphs in initial and final smoothed designs

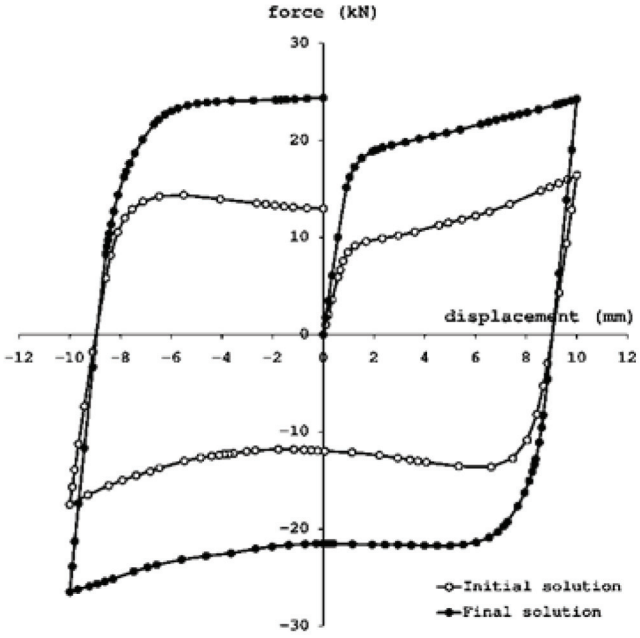

eigenfrequencies of a structure away from a given excitation frequency.

Topology optimization of structures under periodic loads has been discussed. An average dynamic compliance measure has been considered as the objective function to be minimized. Sensitivities of this objective function have been computed. Numerical examples have been solved to illustrate the applications of the optimization method. Topology design of structures under a combination of periodic (and static) loads with different frequencies has been addressed. This is of practical importance, for example when a periodic load is expanded using Fourier series.

Issues and difficulties of considering the non-linear material and geometry behavior of the system have been briefly discussed. The sensitivities of eigenfrequencies and dynamic

compliance of structures in presence of damping have been derived.

The BESO technique has been modified and used to maximize the energy absorption of a passive metallic damper. Sensitivity analysis of the non-linear system has been presented. Simple approaches to achieve shape optimization and periodic solutions have been addressed. It has been illustrated that the optimized solution not only provides higher energy absorption capacities but also offers smoother stress distribution resulting in better fatigue resistance.

It has been shown that in seismic design of structures, topology optimization techniques can be useful in both conceptual design of structural systems (e.g. maximization of fundamental frequency of a frame) and detailed design of structural members (e.g. maximization of energy absorption of passive dampers). These techniques are capable of dealing with different objective functions and different material models.

REFERENCES

Bendsøe, M. P. (1989). Optimal shape design as a material distribution problem. *Structural Optimization*, *1*(4), 193–202. doi:10.1007/BF01650949

Bendsøe, M. P., & Kikuchi, N. (1988). Generating optimal topologies in structural design using a homogenization method. *Computer Methods in Applied Mechanics and Engineering*, *71*(2), 197–224. doi:10.1016/0045-7825(88)90086-2

Bendsøe, M. P., & Sigmund, O. (1999). Material interpolation schemes in topology optimization. *Archive of Applied Mechanics*, *69*(9–10), 635–654.

Bendsøe, M. P., & Sigmund, O. (2003). *Topology optimization - Theory, methods, and applications*. Berlin, Germany: Springer.

Beyer, H.-G., & Sendhoff, B. (2007). Robust optimization – A comprehensive survey. *Computer Methods in Applied Mechanics and Engineering*, *196*(33–34), 3190–3218. doi:10.1016/j.cma.2007.03.003

Bratus, A. S., & Seyranian, A. P. (1983). Bimodal solutions in eigenvalue optimization problems. *Journal of Applied Mathematics and Mechanics*, *47*(4), 451–457. doi:10.1016/0021-8928(83)90081-3

Buhl, T., Pedersen, C. B. W., & Sigmund, O. (2000). Stiffness design of geometrically nonlinear structures using topology optimization. *Structural and Multidisciplinary Optimization*, *19*(2), 93–104. doi:10.1007/s001580050089

Chan, R. W. K., & Albermani, F. (2008). Experimental study of steel slit damper for passive energy dissipation. *Engineering Structures*, *30*(4), 1058–1066. doi:10.1016/j.engstruct.2007.07.005

Chopra, A. K. (1995). *Dynamics of structures – Theory and applications to earthquake engineering*. Upper Saddle River, NJ: Prentice Hall International.

Cox, S. J., & Overton, M. L. (1992). On the optimal design of columns against buckling. *SIAM Journal on Mathematical Analysis*, *23*(2), 287–325. doi:10.1137/0523015

Culmann, K. (1866). *Die graphische Statik*. Zürich, Switzerland: Mayer und Zeller.

Díaz, A. R., & Kikuchi, N. (1992). Solutions to shape and topology eigenvalue optimization problems using a homogenization method. *International Journal for Numerical Methods in Engineering*, *35*(7), 1487–1502. doi:10.1002/nme.1620350707

Du, J., & Olhoff, N. (2007). Topological design of freely vibrating continuum structures for maximum values of simple and multiple eigenfrequencies and frequency gaps. *Structural and Multidisciplinary Optimization*, *34*(2), 91–110. doi:10.1007/s00158-007-0101-y

Elnashai, A. S., & Chryssanthopoulos, M. (1991). Effect of random material variability on seismic design parameters of steel frames. *Earthquake Engineering & Structural Dynamics*, *20*(2), 101–114. doi:10.1002/eqe.4290200202

Ghabraie, K., Chan, R., Huang, X., & Xie, Y. M. (2010). Shape optimization of metallic yielding devices for passive mitigation of seismic energy. *Engineering Structures*, *32*(8), 2258–2267. doi:10.1016/j.engstruct.2010.03.028

Haug, E. J., & Rousselet, B. (1980). Design sensitivity analysis in structural mechanics. II: Eigenvalue variations. *Journal of Structural Mechanics*, *8*(2), 161–186. doi:10.1080/03601218008907358

Huang, X., & Xie, Y. M. (2007). Convergent and mesh-independent solutions for the bi-directional evolutionary structural optimization method. *Finite Elements in Analysis and Design*, *43*(14), 1039–1049. doi:10.1016/j.finel.2007.06.006

Huang, X., & Xie, Y. M. (2008). Topology optimization of nonlinear structures under displacement loading. *Engineering Structures*, *30*(7), 2057–2068. doi:10.1016/j.engstruct.2008.01.009

Huang, X., Xie, Y. M., & Lu, G. (2007). Topology optimization of energy-absorbing structures. *International Journal of Crashworthiness*, *12*(6), 663–675. doi:10.1080/13588260701497862

Huang, X., Zuo, Z. H., & Xie, Y. M. (2010). Evolutionary topological optimization of vibrating continuum structures for natural frequencies. *Computers & Structures*, *88*(5–6), 357–364. doi:10.1016/j.compstruc.2009.11.011

Jensen, J. S. (2007). Topology optimization of dynamics problems with Padé approximants. *International Journal for Numerical Methods in Engineering*, *72*(13), 1605–1630. doi:10.1002/nme.2065

Jog, C. S. (2002). Topology design of structures subjected to periodic loading. *Journal of Sound and Vibration*, *253*(3), 687–709. doi:10.1006/jsvi.2001.4075

Jung, D., & Gea, H. C. (2004). Topology optimization of nonlinear structures. *Finite Elements in Analysis and Design*, *40*(11), 1417–1427. doi:10.1016/j.finel.2003.08.011

Karush, W. (1939). *Minima of functions of several variables with inequalities as side constraints*. Master's thesis, Department of Mathematics, University of Chicago, Chicago, Illinois.

Kharmanda, G., Olhoff, N., Mohamed, A., & Lemaire, M. (2004). Reliability-based topology optimization. *Structural and Multidisciplinary Optimization*, *26*(5), 295–307. doi:10.1007/s00158-003-0322-7

Kosaka, I., & Swan, C. C. (1999). A symmetry reduction method for continuum structural topology optimization. *Computers & Structures*, *70*(1), 47–61. doi:10.1016/S0045-7949(98)00158-8

Kuhn, H. W., & Tucker, A. W. (1951). Nonlinear programming. In *Proceedings of 2nd Berkeley Symposium* (pp. 481–492). Berkeley, CA: University of California Press.

Kuwamura, H., & Kato, B. (1989). Effects of randomness in structural members' yield strength on the structural systems' ductility. *Journal of Constructional Steel Research*, *13*(2–3), 79–93. doi:10.1016/0143-974X(89)90007-2

Lund, E. (1994). *Finite element based design sensitivity analysis and optimization*. Unpublished doctoral dissertation, Institute of Mechanical Engineering, Aalborg University, Denmark.

Ma, Z. D., Cheng, H. C., & Kikuchi, N. (1995). Topological design for vibrating structures. *Computer Methods in Applied Mechanics and Engineering*, *121*(1–4), 259–280. doi:10.1016/0045-7825(94)00714-X

Ma, Z. D., Kikuchi, N., & Hagiwara, I. (1993). Structural topology and shape optimization for a frequency response problem. *Computational Mechanics*, *13*(3), 157–174. doi:10.1007/BF00370133

Maeda, Y., Nishiwaki, S., Izui, K., Yoshimura, M., Matsui, K., & Terada, K. (2006). Structural topology optimization of vibrating structures with specified eigenfrequencies and eigenmode shapes. *International Journal for Numerical Methods in Engineering*, *67*(5), 597–628. doi:10.1002/nme.1626

Michell, A. G. M. (1904). The limits of economy of material in frame structures. *Philosophical Magazine*, *6*(8), 589–597.

Min, S., Kikuchi, N., Park, Y. C., Kim, S., & Chang, S. (1999). Optimal topology design of structures under dynamic loads. *Structural Optimization*, *17*(2–3), 208–218.

Oh, S. H., Kimb, Y. J., & Ryu, H. S. (2009). Seismic performance of steel structures with slit dampers. *Engineering Structures*, *31*(9), 1997–2008. doi:10.1016/j.engstruct.2009.03.003

Olhoff, N., & Du, J. (2005). Topological design of structures subjected to forced vibration. In J. Herskovits (Ed.), *Proceedings of the 6th World Congress of Structural and Multidisciplinary Optimization*, Rio de Janeiro, Brazil, 30 May–03 June.

Olhoff, N., & Rasmussen, S. H. (1977). On single and bimodal optimum buckling loads of clamped columns. *International Journal of Solids and Structures*, *13*(7), 605–614. doi:10.1016/0020-7683(77)90043-9

Overton, M. L. (1992). Large-scale optimization of eigenvalues. *SIAM Journal on Optimization*, *2*(1), 88–120. doi:10.1137/0802007

Papadrakakis, M., Lagaros, N. D., & Plevris, V. (2005). Design optimization of steel structures considering uncertainties. *Engineering Structures*, *27*(9), 1408–1418. doi:10.1016/j.engstruct.2005.04.002

Pedersen, N. L. (2000). Maximization of eigenvalues using topology optimization. *Structural and Multidisciplinary Optimization*, *20*(1), 2–11. doi:10.1007/s001580050130

Prager, W. (1969). *Optimality criteria derived from classical extermum principles. Technical report, SM Studies Series*. Ontario, Canada: Solid Mechanics Division, University of Waterloo.

Prager, W. (1974). A note on discretized Michell structures. *Computer Methods in Applied Mechanics and Engineering*, *3*(3), 349–355. doi:10.1016/0045-7825(74)90019-X

Querin, O. M. (1997). *Evolutionary structural optimisation stress based formulation and implementation*. Unpublished Doctoral dissertation, Department of Aeronautical Engineering, University of Sydney, Sydney, Australia.

Querin, O. M., Steven, G. P., & Xie, Y. M. (1998). Evolutionary structural optimisation (ESO) using a bidirectional algorithm. *Engineering Computations*, *15*(8), 1031–1048. doi:10.1108/02644409810244129

Rozvany, G. I. N. (1972a). Grillages of maximum strength and maximum stiffness. *International Journal of Mechanical Sciences*, *14*(10), 651–666. doi:10.1016/0020-7403(72)90023-9

Rozvany, G. I. N. (1972b). Optimal load transmission by flexure. *Computer Methods in Applied Mechanics and Engineering*, *1*(3), 253–263. doi:10.1016/0045-7825(72)90007-2

Rozvany, G. I. N., Zhou, M., & Birker, T. (1992). Generalized shape optimization without homogenization. *Structural Optimization*, *4*(3–4), 250–252. doi:10.1007/BF01742754

Seyranian, A. P., Lund, E., & Olhoff, N. (1994). Multiple eigenvalues in structural optimization problems. *Structural and Multidisciplinary Optimization*, *8*(4), 207–227.

Sigmund, O., & Petersson, J. (1998). Numerical instabilities in topology optimization: A survey on procedures dealing with checkerboards, mesh dependencies and local minima. *Structural and Multidisciplinary Optimization*, *16*(1), 68–75.

Soong, T. T., & Spencer, B. F. Jr. (2002). Supplemental energy dissipation: State-of-the-art and state-of-the-practice. *Engineering Structures*, *24*(3), 243–259. doi:10.1016/S0141-0296(01)00092-X

Svanberg, K. (1987). The method of moving asymptotes—A new method for structural optimization. *International Journal for Numerical Methods in Engineering*, *24*(2), 359–373. doi:10.1002/nme.1620240207

Xie, Y. M., & Steven, G. P. (1993). A simple evolutionary procedure for structural optimization. *Computers & Structures*, *49*(5), 885–896. doi:10.1016/0045-7949(93)90035-C

Xie, Y. M., & Steven, G. P. (1996). Evolutionary structural optimization for dynamic problems. *Computers & Structures*, *58*(6), 1067–1073. doi:10.1016/0045-7949(95)00235-9

Yang, X. Y., Xie, Y. M., Steven, G. P., & Querin, O. M. (1999a). Bidirectional evolutionary method for stiffness optimization. *American Institute of Aeronautics and Astronautics Journal*, *37*(11), 1483–1488.

Yang, X. Y., Xie, Y. M., Steven, G. P., & Querin, O. M. (1999b). Topology optimization for frequencies using an evolutionary method. *Journal of Structural Engineering*, *125*(12), 1432–1438. doi:10.1061/(ASCE)0733-9445(1999)125:12(1432)

Yoon, G. H. (2010a). Maximizing the fundamental eigenfrequency of geometrically nonlinear structures by topology optimization based on element connectivity parameterization. *Computers & Structures*, *88*(1–2), 120–133. doi:10.1016/j.compstruc.2009.07.006

Yoon, G. H. (2010b). Structural topology optimization for frequency response problem using model reduction schemes. *Computer Methods in Applied Mechanics and Engineering*, *199*(25–28), 1744–1763. doi:10.1016/j.cma.2010.02.002

Yoon, G. H. (2011). Topology optimization for nonlinear dynamic problem with multiple materials and material-dependent boundary condition. *Finite Elements in Analysis and Design*, *47*(7), 753–763. doi:10.1016/j.finel.2011.02.006

Yoon, G. H., & Kim, Y. Y. (2005). Element connectivity parameterization for topology optimization of geometrically nonlinear structures. *International Journal of Solids and Structures*, *42*(7), 1983–2009. doi:10.1016/j.ijsolstr.2004.09.005

Zhao, C. B., Steven, G. P., & Xie, Y. M. (1997). Evolutionary optimization of maximizing the difference between two natural frequencies of a vibrating structure. *Structural Optimization*, *13*(2–3), 148–154. doi:10.1007/BF01199234

Zhou, M., & Rozvany, G. I. N. (2001). On the validity of ESO type methods in topology optimization. *Structural and Multidisciplinary Optimization*, *21*(1), 80–83. doi:10.1007/s001580050170

Zienkiewicz, O. C., Taylor, R. L., & Zhu, J. Z. (2005). *The finite element method: Its basis and fundamentals*. Oxford, UK: Elsevier Butterworth-Heinemann.

KEY TERMS AND DEFINITIONS

Compliance Minimization: In structural optimization under static loads, minimizing the mean compliance is equivalent to maximizing the structural stiffness. Under dynamic loads, the average of mean compliance over a cycle can be considered as an objective function.

Eigenfrequency Control: Topology optimization techniques can be used to increase or decrease any of natural frequencies of a structural system.

Passive Dampers: These devices are used to enhance the energy dissipation capability of structural systems to mitigate seismic hazard.

Sensitivity Analysis: In solving an optimization problem, finding the derivatives of the objective function with respect to the design variables is sometimes referred to as sensitivity analysis.

Shape Optimization: Finding the best shape of the elements of a structural system in which the overall layout, topology and connectivity of the elements is previously determined is known as shape optimization.

Sizing Optimization: Finding the optimum dimensions of the elements in a structural system when the overall layout, connectivity and shape of the elements are fixed is termed as sizing optimization.

Topology Optimization: The problem of finding the best topology and layout of the elements of a structural system is known as topology optimization.